TITLE PAGE

Protective concentric cardiac proteostasis adaptations to chronic cAMP-stress at young ages wanes in advanced age leading to accelerated cardiac aging

*Maria Grazia Perino PhD[1], *Miguel Calvo-Rubio Barrera PhD[2], Giulio Agnetti PhD[3], Mark Ranek PhD[3], Daniel R. Riordon BS[1], Christopher H. Morrell PhD[1], Khalid Chakir PhD[1], Jia-Hua Qu PhD[4], Kirill V Tarasov PhD[1], Edward G. Lakatta MD[1]

Correspondence to: Maria Grazia Perino, PhD, Laboratory of Cardiovascular Science, National Institute on Aging, National Institutes of Health, 251 Bayview Blvd, Baltimore (MD) 21224, United States, Email: mariagrazia.perino@nih.gov

Affiliations:

[1]Laboratory of Cardiovascular Science, National Institute on Aging, National Institutes of Health, Baltimore, United States

[2]Translational Gerontology Branch, Intramural Research Program, National Institute on Aging, National Institutes of Health, Baltimore, United States

[3]Division of Cardiology, Department of Medicine, Johns Hopkins University School of Medicine, Baltimore, United States

[4]University of California, San Francisco - School of Medicine

*Contributed equally

Total word count: 9309

ABSTRACT

BACKGROUND: Deregulated proteostasis leading to accumulation of misfolded proteins, electron-dense aggregates (lipofuscin, LF), desmin preamyloid oligomers (PAOs), and proteotoxic stress is a hallmark of aging. Here, we investigate changes in proteostasis with aging, in the context of a chronic cardiac cyclic adenosine monophosphate (cAMP)-dependent stress in a mouse model with specific cardiac over-expression of adenylyl cyclase VIII (TG^{AC8}).

METHODS: Protein quality control (PQC) mechanisms (ubiquitin proteasome system (UPS) and autophagy), including mitophagy, were evaluated in left ventricles (LVs) at young age (3-4 months) and later in life (18-21 months). Autophagy flux was measured in response to the lysosomotropic drug chloroquine (CQ). Protein synthesis was assessed according to the SUnSET method (puromycin).

RESULTS: At 3 months of age, established autophagy markers such as the microtubule-associated protein 1 light chain 3 (LC3), p62, and their phospho-forms were modulated accordingly to a scenario of more efficient autophagy, with a faster flux. Lysosome performance (cathepsin L1 activity) was also significantly increased, confirming higher cargo degradation capacity and upregulated proteostasis at 3 months. With age, however, a maladaptive marker-specific accelerated flux (LC3A, p62), in the context of a slower autophagy flux, led to aggresome buildup. Furthermore, although the mitophagy receptors PARKIN, p62-S403, p62-S349, and FKBP8 remained all upregulated, old TG^{AC8} mice markedly portrayed a phenotype with impaired mitophagy, accumulation of

lipofuscin (LF) bodies of aberrant sizes and brownish-to black pigment. Finally, cardiac preamyloid oligomers (PAOs) were significantly increased, and the structural protein desmin, cleaved and tagged for ubiquitination. In contrast, protein synthesis decreased as occurs in normal aging.

CONCLUSIONS: Our findings indicate that proteostasis maintains cardiac health at young age (3-4months), but a lifetime exposure to chronic pathophysiologic states that increase cardiac ubiquitination and stress, by sustained activation of the AC/cAMP/PKA/Ca^{2+} axis, more severely dysregulate proteostasis, compared to normal aging, ultimately leading to proteostasis insufficiency, and accelerated cardiac aging.

GRAPHIC ABSTRACT: A graphic abstract is available for this article.

Key Words: proteostasis, cardiac stress, chloroquine, mitophagy, aging

Nonstandard Abbreviations and Acronyms

LF lipofuscin

PAOs preamyloid oligomers

cAMP cyclic adenosine monophosphate

AC adenylyl cyclase

AC8 adenylyl cyclase VIII

PQC protein quality control

UPS ubiquitin proteasome system

CQ chloroquine

70 **LC3** microtubule-associated protein 1 light chain 3

71 **LV** left ventricle

72 **HF** heart failure

73 **PE** phosphatidylethanolamine

74 **PKA/PKC** protein kinase A/ protein kinase C

75 **KEAP1** Kelch-like ECH-associated protein 1

76 **NRF2** transcription factor NF-E2-related factor 2

77 **ACP2** lysosomal acid phosphatase

78 **ATG4B** autophagy related 4B cysteine peptidase

79 **TEM** transmission electron microscopy

80 **ROS** reactive oxygen species

81

82 # INTRODUCTION

83 Cardiac proteostasis, the balance of protein synthesis, and degradation, is required
84 maintenance for cardiac health. Pathogenic aspects of protein misfolding and aggregation
85 are collectively referred to proteotoxicity, and a proteotoxic insult that accompanies
86 advanced age, can ultimately lead to heart dysfunction[1], and eventually, cardiac failure[2].
87 Many protein aggregate–based diseases in the cardiac system, are well characterized[3].
88 Plaque deposition (amyloidosis) or accumulation of soluble, oligomeric "aggresomes",
89 and, recently, desmin disorganization with aging and the existence in the heart of desmin
90 preamyloid oligomers (PAOs)[4], have also emerged as a common hallmark of acquired
91 heart failure (HF)[5,6,7].

92 Many factors can lead to proteostatic collapse, including the imbalance in protein
93 synthesis and degradation, exhaustion of the proteostasis machinery, and
94 downregulation of clearing mechanisms, such as the ubiquitin proteasome system (UPS)
95 and autophagy[8]. Impaired autophagy and mitophagy with age, due to reduced lysosomal[9]
96 and mitochondrial fitness by increased oxidative stress[10], have been linked to the
97 accumulation of electron-dense aggregates, generally referred to lipofuscin (LF)
98 accumulation. As age advances, proteostasis mechanisms begin to collapse[11], and
99 deficient breakdown of damaged proteins and organelles may lead to accumulation of LF,
100 which linearly associates with age, and is inversely correlated with longevity[12,13]

101 Marked chronic catecholamine-induced cardiac stress leads to heart failure[14,15]. Our
102 recent study demonstrated that in response to chronic severe cardiac stress by over-
103 expression of adenylyl cyclase VIII (AC8) in mice (TG^{AC8}), induced concentric adaptation
104 circuitry at young age (3-4 months), including upregulation of protein synthesis and

105 degradation mechanism (proteasome and autophagy) to protect against stress[16],
106 maintained a remarkable, hyperdynamic cardiac phenotype for up to about one year of
107 age[17-20]. Then, signs of chronic heart failure (CHF) emerged and cardiomyopathy
108 ensued[20-22]. Here we evaluate proteostasis mechanisms induced by exposure to severe
109 sustained cAMP-dependent chronic cardiac stress with aging, compared to normal aging.

110 # METHODS

111 **Experimental animals**

112 All studies were performed in accordance with the Guide for the Care and Use of
113 Laboratory Animals published by the National Institutes of Health (NIH Publication no. 85-
114 23, revised 1996). The experimental protocols were approved by the Animal Care and
115 Use Committee of the National Institutes of Health (protocol #441-LCS-2019). A breeder
116 pair of TG^{AC8} over expression mice (background strain C57BL/6 from Jackson Labs,
117 Stock # 000664), where the cDNA coding for human TG^{AC8} is expressed under the murine
118 α-myosin heavy chain (α-MHC) promoter, was a gift from Nicole Defer/Jacques Hanoune,
119 Unite de Recherches, INSERM U- 99, Hôpital Henri Mondor, F-94010 Créteil, France[17].

120 Mice were bred at 3 months of age and housed in a climate-controlled room with 12-
121 hour light cycle and free access to food and water, as previously described[14]. All assays
122 were performed in 3-4-month-old (young) and 17-21-month-old (old) males and compared
123 to age-matched wild-type (WT) littermates. Animals were sacrificed using
124 Ketamine/Xylazine mixture, by intraperitoneal (IP) administration, in accordance with the
125 approved protocol (#441-LCS-2019).

126 **Heart and cardiac tissue isolation**

127 Following Ketamine/Xylazine mixture intraperitoneal (IP) administration, the heart was
128 quickly removed and placed into cold PBS solution. The left ventricle (LV) free wall,
129 without the septum, was identified anatomically, under a dissecting microscope, and
130 pieces of tissue 2x3 mm were dissected and snap-frozen in liquid nitrogen.

131 **Protein extraction and WB**

132 Flash frozen tissue was homogenized as previously[16]. Briefly, snap-frozen left
133 ventricle (LV) tissue from 3-month-old and 21-month-old mice was homogenized and
134 lysed in ice cold RIPA buffer (Thermo Fisher Scientific: 25 mM Tris-HCl (pH 7.6), 150 mM
135 NaCl, 1% NP-40, 1% sodium deoxycholate, 0.1% SDS) supplemented with a Halt
136 protease inhibitor cocktail (Thermo Fisher Scientific), Halt phosphatase inhibitor cocktail
137 (Thermo Fisher Scientific) and 1 mM phenylmethyl sulfonyl fluoride, using a Precellys
138 homogenizer (Bertin Instruments) with tissue homogenization kit CKMix (Bertin
139 Instruments) at 4°C. Extracts were then centrifuged at 10,000g for 10 min at 4°C and the
140 protein concentration of the soluble fraction determined using the Bicinchoninic Acid
141 (BCA) Assay (Thermo Fisher Scientific). Samples were denatured in 4X Laemmli sample
142 buffer (BioRad Laboratories) containing 355 mM 2-mercaptoethanol at 95°C for 5 min, or
143 DTT at 70°C for 10 min, and proteins (25µg/lane) were resolved on 4-20% Criterion TGX
144 Stain Free gels (Bio-Rad Laboratories) by SDS/PAGE. To induce crosslinking of Stain
145 Free gel trihalo compound with protein tryptophan residues gels were exposed to UV
146 transillumination for 2-3 mins. Proteins were then transferred to low fluorescence
147 polyvinylidene difluoride (LF-PVDF) membranes (BioRad Laboratories) using an
148 electrophoretic transfer cell (Mini Trans-Blot, Bio-Rad). Membrane total protein was
149 visualized using an Amersham Imager 600 (AI600) (GE Healthcare Life Sciences) with

150 UV transillumination to induce and capture a fluorescence signal. Blocked membranes
151 (5% milk/tris-buffered saline with Tween-20, TBST) were incubated with the primary
152 antibodies indicated in the **Major Resource Table**. Primary antibodies were then
153 detected using horseradish peroxidase (HRP) conjugated antibody (Invitrogen) at
154 1:5,000, and bands were visualized using Pierce SuperSignal West Pico Plus ECL
155 substrate kits (Thermo Scientific), the signal captured using an Amersham Imager 600
156 (AI600) (GE Healthcare Life Sciences) and quantified using ImageQuant TL software (GE
157 Healthcare Life Sciences). Band density was normalized to total protein, and TG^{AC8} to
158 average of WT.

159 **Protein aggregation assay**

160 Proteostat kit (Enzo Life Science, ENZ-51023) was used to measure protein
161 aggregates, as previously published[16], following the manufacturer's instructions.
162 Specifically, 10 µg of protein were loaded into a 96-well microplate, and background
163 readings were subtracted from sample recordings.

164 **Cathepsin L1 activity assay**

165 Cathepsin L1 activity was measured using the fluorimetric kit (Abcam, ab65306)
166 according to the manufacturer's instructions. Briefly, snap-frozen left ventricles (LV)
167 stored at -80°C were thawed on ice, and 10 mg of tissue was resuspended in 50 µl of CL
168 Buffer, then homogenized with a Dounce homogenizer sitting on ice, with 10–15 passes.
169 Samples were centrifuged for 2–5 mins at 4°C at top speed using a cold microcentrifuge
170 to remove any insoluble material, then supernatants were collected and transferred to a
171 clean tube, on ice. Activity was performed at different dilutions to reach Vmax, in the
172 presence of Ac-FR-AFC fluorogenic substrate (200 µM final concentration), at 37°C for
173 1–2 hours, at an excitation wavelength of 400 nm and an emission wavelength of 505 nm

174 using the Cytation 5 microplate reader (Biotek). Fold-increase in Cathepsin L activity was
175 determined by comparing the relative fluorescence units (RFU) with the level of the
176 uninduced control, after subtraction of the negative control sample. TG^{AC8} values were
177 normalized to average of WT.

178 **Transmission Electron Microscopy (TEM)**

179 Left ventricles (LVs) for transmission electron microscopy were fixed using 2.5%
180 glutaraldehyde in 0.1 M sodium cacodylate buffer, pH 7. Samples were post-fixed in 1%
181 osmium tetroxide for 1 h at 4°C in the same buffer, dehydrated, and then embedded in
182 Embed 812 resin (Electron Microscopy Sciences, Hatfield, PA) through a series of resin
183 resin-propylene oxide gradients to pure resin. Blocks were formed in fresh resin contained
184 in silicon molds, and the resin was polymerized for 48-72 h at 65°C; blocks were then
185 trimmed and sectioned in an EM UC7 ultramicrotome (Leica Microsystems, Buffalo
186 Grove, IL) to obtain both semi-thick (0.5-1 µm width) and ultrathin (40-60 nm width)
187 sections. Semi-thick sections were mounted on glass slides and stained with 1% toluidine
188 blue in a 1% borax aqueous solution for 2 min. Palade-stained (OsO4) and Toluidine blue-
189 stained semi-thick sections were then imaged using a Leica AXIO Imager light
190 microscope with a 63x oil immersion objective, for quality control and Lipofuscin (LF)
191 quantification. Ultrathin sections were stained with uranyl acetate and lead citrate and
192 then imaged on a Talos L120C Transmission Electron Microscope (TEM) with a 4K Ceta
193 CMOS camera, for macroautophagic events quantification.

194 Micrographs at ×2000 x5000 and x11000 magnification were obtained from randomly
195 selected cytoplasmic areas of cardiomyocytes, for illustration purposes and quantitative
196 analysis of macroautophagic events population. Two stereological parameters were
197 determined: (a) the numerical profile density Na (number of figures of interest / µm2 of

198 cell fraction), and (b) volume density of figures of interest (Vv; i.e., the volume fraction of
199 cardiomyocyte cytoplasm occupied by figures of interest). Volume density was obtained
200 following a point analysis using a simple square lattice test system[23], with superposition
201 of a virtual grid over the micrographs where the user performs a point-counting method.
202 Autophagosomes were identified as double-membrane vesicles with identifiable cargo
203 and comparable density to the surrounding cytosol. Autolysosomes and residual bodies
204 were denoted as single membrane vesicles containing non-identifiable cargo of higher
205 density than the surrounded cytosol and fragmented organelles.

206 Lipofuscin bodies were identified following Palade staining[24] by the presence of
207 densely packed lipids with a dark brown-black color against cardiomyocyte cytosol, which
208 allowed a straightforward segmentation of the image and posterior quantification of the
209 planimetric and stereological parameters. Point counting and areas of vesicles and
210 cytosol were measured using manual tracking with ImageJ software by a blinded
211 investigator.

212 **Quantification of desmin preamyloid oligomers (PAOs)**

213 Myofilament-enriched, insoluble fractions were prepared as described previously[7].
214 Fractions were separated using precast NuPAGE gels (Thermo Fisher Scientific) with
215 MES buffer, and probed with the desmin antibody (DE-U-10, Sigma, 1:10,000) or the A11
216 antibody (kindly provided by Dr. Charles Glabe at UC Irvine[25], 1:1,500). TG^{AC8} values
217 were normalized to WT.

218 **Statistics**

219 Data are presented as median ± range or median ± interquartile range. Representative
220 TEM images and western blots were chosen based on the resemblance to the average
221 values. Number of samples per group are indicated in each legend. Statistical analyses

222 were performed in GraphPad Prism 9. ROUT analyses were applied to identify outliers,
223 which were excluded from group comparison analyses. Student *t* test with Welch's
224 correction was used to compare data between 2 groups. Two-way ANOVA followed by
225 Original FDR method of Benjamini and Hochberg was used for multiple comparisons[26].
226 For datasets with matching LC3I and LC3II from the same animal, a multiple measures
227 approach with three-way mixed ANOVA or mixed-effect analysis for repeated measures,
228 followed by Original FDR method of Benjamini and Hochberg, was taken. A q-value or
229 individual p-value <0.05 was considered statistically significant. * Indicates differences
230 between genotypes (WT vs TG^{AC8}), # indicates differences between treatments (CQ vs
231 saline), $ indicates differences between ages (young vs old).

232 # RESULTS

233 **Autophagy is upregulated in young TG^{AC8} heart**

234 To assess basal autophagy in left ventricle (LV) in the young (3-4 months) TG^{AC8} and
235 WT, we performed WB of the established autophagy markers LC3 and p62, and assessed
236 their phosphorylation state, which affects their activity. Significant changes in the
237 modulation of the cytosolic LC3I and its lipidated product LC3II (LC3-PE), the latter
238 recruited to the autophagosomal membrane during autophagy, were evident in TG^{AC8} vs
239 WT. Specifically, LC3**AI** was significantly upregulated, in TG^{AC8} vs WT, whereas LC3**AII**
240 was unchanged (Figure 1A); in contrast, cytosolic LC3**BI** did not change in TG^{AC8},
241 whereas lipidated LC3**BII** was significantly downregulated, compared to WT (Figure 1B).
242 Their ratios (LC3II/LC3I), an indication of autophagy induction/activation, and of LC3
243 processing efficiency, also differed between genotypes. Specifically, they were
244 significantly decreased in TG^{AC8} for both isoforms, compared to WT (Figures 1C, 1D) due

245 to upregulation of LC3**AI** and downregulation of LC3**BII**, respectively. Moreover,
246 phosphorylation of LC3, inhibitory when at S12[27] and stimulatory when at T50[28], was half
247 (Figure 1E) or 1.3-fold significantly increased (Figure 1F), respectively, in TG^{AC8} vs WT,
248 suggesting the existence of more favorable autophagy conditions in the young TG^{AC8}.

249 Total p62 expression was significantly upregulated in TG^{AC8} vs WT (Figure 2A), as
250 was p62 phosphorylation at S403 (p62-S403) (Figure 2B) and at S349 (p62-S349) (Figure
251 2C); the ratios of phospho-proteins at both sites to total p62 protein (Figure 2D, 2E), were
252 also significantly increased, indicating higher "aggresome" disposal (p62-S403 has higher
253 affinity to ubiquitylated cargo, including ubiquitinated/depolarized mitochondria), and
254 activation of defense mechanisms from oxidative stress (p62-S349) in the TG^{AC8} heart,
255 at 3-4 months of age.

256 In summary, upregulation of key markers of selective autophagy (clearance and
257 activation of protection mechanisms from oxidative stress) maintains heart health of
258 young TG^{AC8}, at a young age, in a context of an increased cardiac workload by chronic
259 cardiac cAMP-derived stress[16].

260 **Lysosomal function is increased and autophagic flux is accelerated in young TG^{AC8}**
261 **heart**

262 Because our previous work has shown that protein levels of lysosomal cathepsins are
263 upregulated in the TG^{AC8}, compared to age-matched WT[16], we quantified relative
264 changes in different cathepsins in the TG^{AC8} LV, compared to WT. Cathepsins Z and S
265 were more enriched in TG^{AC8}, whereas cathepsin L1 showed the least significant change
266 (Figure 3A, Table S1). We next assessed lysosome function by measuring cathepsin L1
267 activity. The activity of L1 was significantly higher in TG^{AC8}, compared to WT (Figure 3B),
268 and this result, paired with WB quantification of the lysosomal acid phosphatase, ACP2,

269 which was also significantly increased (Figure 3C), suggested an overall higher lysosomal
270 fitness (function) in TG^{AC8}, compared to WT.

271 Since autophagy is a dynamic, multi-steps process, our next step was to evaluate how
272 the young TG^{AC8} heart is handling the cargo, from uptake to disposal. We measured
273 autophagy flux by inhibiting the lysosome with chloroquine (CQ), in non-fasting conditions
274 to specifically evaluate changes in basal autophagy (without starvation). In WT, following
275 CQ treatment, no changes were noticeable in LC3 and p62 (Figures 4A-D, Figure 4E), as
276 expected, because basal autophagy is normally undetectable; in contrast, in the TG^{AC8}
277 both LC3**AI** and LC3**BI** (Figures 4A, 4B) and p62 protein levels (Figure 4E) became
278 significantly reduced following CQ treatment, compared to saline, whereas LC3**AII** and
279 LC3**BII** remained unchanged. Thus, following CQ, LC3II/LC3I ratios (both A and B
280 isoforms) (Figures 4C, 4D) significantly increased in TG^{AC8}, compared to saline.

281 We next employed transmission electron microscopy (TEM) to directly visualize
282 autophagy figures in TG^{AC8} vs WT in the contest of saline vs CQ treatment. Results
283 showed a significant increase in the number of early and late autophagic events (Figure
284 4F, 4G) in TG^{AC8} vs WT, demonstrating that basal autophagy differs between the two
285 genotypes, and that autophagy flux is accelerated in TG^{AC8}. Therefore, an accelerated
286 autophagic flux and an increase in lysosome performance ensures effective clearance of
287 misfolded proteins, preventing excessive garbage accumulation in the young (3-4
288 months) TG^{AC8} heart, in the context of increased cardiac workload and other cardiac
289 protection circuitry at this age[16], in induced chronic activation of the AC/cAMP/PKA/Ca^{2+}
290 axis.

291 **Accelerated autophagic flux in young TG^{AC8} heart becomes maladaptive and**
292 **insufficient in old age**

293 Because autophagy induction and clearance have been shown to decrease with
294 aging[9], we assessed by WB LC3 and ATG4B (involved in LC3 turnover)[29] in young (3-
295 month-old) and aged (20-21-month-old) TG^{AC8} LVs and age-matched WT. Both markers
296 were significantly downregulated with aging (Figures 5A, 5B, Figure S1), with specific
297 accumulation of LC3II (Figures 5A, 5B), compared to young animals. Upregulated levels
298 of LC3II with aging, increased LC3II/LC3I ratios in both isoforms indicating aging as the
299 main effect (Figures 5C, 5D, S2i, S2ii).

300 Paired TEM micrograph analysis (planimetry and stereology) showed a significant
301 age-associated decrease in event flux in *early* stages of autophagy (Figures 5E, 5I); in
302 contrast, *late*-stage event flux was increased (Figures 5H, 5I). This results, taken together
303 with the accumulation of lipidated LC3II, confirm an age-accelerated downregulation of
304 autophagy induction and an impaired cargo clearance, regardless of genotype.

305 We next focused on autophagy and cargo disposal between the old (19-21-month)
306 TG^{AC8} and age-matched WT, specifically we assessed by WB LC3 states (including
307 phosphorylation) and measured autophagic flux. Interestingly, LC3**AI** levels were
308 significantly upregulated in old TG^{AC8} compared to age-matched WT (Figures 6A), (similar
309 to the genotype difference in LC3**AI** expression at 3-month (Figure 1A)), while LC3**AII** <u>did
310 not significantly differ by genotype</u>. Thus, LC3AII/LC3AI ratio was decreased in old TG^{AC8}
311 vs WT (Figure S3i). In contrast, LC3**BI** and LC3**BII** (Figures 6B), and LC3BII/LC3BI ratio
312 (Figure S3ii) <u>did not significantly differ by genotype</u>, at old age. Furthermore, LC3
313 phosphorylation (S12 and T50) and ACP2 protein levels (Figure S4) <u>did not differ by
314 genotype</u> at 21-month of age. Taken together, these results indicate that autophagy

315 declines with age, regardless of genotype, and autophagic insufficiency is greater in
316 TG^{AC8} than in WT. As expected, autophagic flux assessment in old WT, showed that LC3
317 and p62 levels did not differ following CQ treatment in non-fasting conditions, similar to
318 results at the young age. In old TG^{AC8}, however, there was a significant accumulation of
319 LC3**AII** following CQ treatment vs WT-CQ (Figure 6A); the LC3AII/LC3AI ratio, did not
320 change following CQ treatment (Figure 6C). Although CQ treatment had no effect on
321 LC3B forms (Figure 6B), LC3BII/LC3BI ratio showed a trend to significantly increase
322 (Figure 6D), demonstrating that LC3 isoform-specific modulation persists in old age, as
323 observed in TG^{AC8} at a young age, previously. Remarkably, and similar to young TG^{AC8}
324 (Figure 4E), p62 expression was significantly downregulated in old TG^{AC8} following CQ,
325 compared to saline (Figure 6E). This result suggests that, although *overall* flux was
326 indeed significantly reduced (Figure 6Fi, 6Fii), stages of autophagic flux involving LC3A
327 and p62 increased significantly in TG^{AC8} in old age.

328 Taken data in figures suggest that, compared to age-matched WT, basal autophagy
329 and autophagic flux of LC3A- and p62 autophagic markers, are accelerated in old TG^{AC8},
330 similar to 3 months of age, but autophagic flux become slower in old age and is clearly
331 insufficient for proper protein and garbage clearance**.**

332 **Proteostasis is more severely deregulated in the old TG^{AC8} heart**

333 Our previous work demonstrated that the ubiquitin proteasome system (UPS) and
334 autophagy, including mitophagy, were all upregulated in the young TG^{AC8}, compared to
335 age-matched WT, indicating cooperation among PQC mechanisms at 3-4 months[16].
336 Although protein synthesis rate was 40% higher in TG^{AC8} vs WT, UPS clearance of these
337 was also upregulated, and insoluble protein “garbage” did not accumulate within cells[16].
338 In addition, the numbers of healthy mitochondria and the percent of cell volume occupied

339 by them, did not differ between TG^{AC8} and WT; in addition, although the canonical cargo
340 receptors PARKIN was significantly upregulated[16], mitochondrial fitness was comparable
341 between genotypes. We here assessed translation rates and PQC mechanisms (UPS
342 activity, aggresomes accumulation, and mitophagy) in aged (19-21-month) TG^{AC8} and
343 age-matched WT.

344 In contrast to the young age, protein synthesis did not differ by genotype in aged mice
345 (Figure 7A). However, translation rates significantly decreased in TG^{AC8}, from 3 to 18-
346 months, a process normally occurring during healthy aging, where decreased energy use
347 and reduced load on the protein quality control machinery, extends life span by sparing
348 proteases and chaperons, directing their activity towards repair of existing proteins rather
349 than the folding of new ones[30-32].

350 We next quantified protein aggregates in 18-month-old mice and age-matched WT.
351 Soluble aggregates accumulated in 18-month TG^{AC8}, compared to age-matched WT
352 (Figure 7B), suggesting that the maladaptive increased autophagic flux, with aging, in old
353 TG^{AC8}, compared to age-matched WT, contributes to deregulated proteostasis.

354 Finally, we evaluated mitophagy signaling pathways in aged (21-month) TG^{AC8} and
355 age-matched WT assessing by WB the expression of specific cargo receptors involved in
356 canonical and non-canonical mitophagy pathways[33]. Specifically, the canonical cargo
357 receptors PARKIN (Figure 7C) and p62-S403 (Figure 7D), recruited to depolarized[34] and
358 polyubitiquinated[35] mitochondria, respectively, and p62-S349 (Figure 7E), upregulated in
359 conditions of oxidative stress[36], were all significantly increased in aged TG^{AC8} compared
360 to age-matched WT, similar to young TG^{AC8}, suggesting activation of canonical
361 mitophagy. Furthermore, the non-canonical cargo receptor FKBP8[37], which assists LC3A

362 during mitophagy and in the clearance of misfolded proteins, was also significantly
363 *upregulated* (Figure 7F) in the old TG^{AC8}, compared to age-matched WT, in contrast to
364 young TG^{AC8} (Figure S5), suggesting the concurrent activation of non-canonical
365 mitophagy in old TG^{AC8}. However, in spite of the upregulation of canonical and non-
366 canonical mitophagy signaling in old TG^{AC8}, staining of semi-thin sections (TEM) still
367 revealed extensive accumulation of undigested material, with disrupted mitochondrial
368 structure in old TG^{AC8} (Figure 7G), indicating a failing mitophagy and upregulated
369 signaling for garbage disposal.

370 These results demonstrate that the TG^{AC8} mouse decreases with aging protein
371 synthesis to preserve energy and focus on repair mechanisms, a process that normally
372 occurs during healthy aging. However, PQC is so inefficient and insufficient in the old
373 TG^{AC8} heart, that leads to more severe age-associated unregulated proteostasis,
374 compared to age-matched WT.

375 **Proteostasis dysregulation in the old TG^{AC8} heart leads to increased lipofuscin**
376 **accumulation and deposition of desmin Pre-Amyloid Oligomers (PAOs)**
377 **contributing to TG^{AC8} accelerated aging**

378 To assess the age-associated proteostasis dysregulation in old TG^{AC8} heart, we
379 evaluated the extent of accumulation of undigested material by performing LF
380 quantification. There was no difference in number (Figure 8A) or average size (Figure 8B)
381 of LF bodies in old TG^{AC8} vs age-matched WT, by semi-thin staining assessment (TEM).
382 However, there was a marked size heterogeneity within the LF population (Figure 8C,
383 8D) in TG^{AC8}, with increased individual LF body' sizes and total volume of LF (Figure 8E)
384 compared to WT, covering in some cases, a big percentage of the cardiomyocyte area
385 (Figure 8F). Interestingly, large aggregates displaying different pigmentation (brownish to

386 black) were only present in TG^{AC8} LVs (Figure 8G), suggesting a different and/or denser
387 composition.

388 Since recent evidence indicates a role of desmin filaments in regulating proteostasis[38],
389 and desmin disorganization has been also documented in the heart[39] as a consequence
390 of accumulation of preamyloid oligomers (PAOs) aggregates, we assessed the
391 contribution of desmin proteotoxicity to the TG^{AC8} heart at the old age (18-month),
392 compared to age-matched WT. TG^{AC8} had significantly higher levels of desmin PAOs
393 (Figure 8H), and a higher percentage of desmin was tagged for ubiquitination (Figure 8Ii),
394 and cleaved (Figure 8Iii), demonstrating severe alteration of the myofilament contractile
395 cardiac machinery in the old TG^{AC8} heart vs age-matched WT.

396 Taken together, accumulation of the age pigment LF, heterogeneity of LF bodies and
397 increased cardiac PAOs, in tandem with the severe disruption in the cardiomyocyte
398 architectural contracting machinery, by desmin disorganization, highly contribute to old
399 TG^{AC8} heart accelerated aging, compared to age-matched WT.

400 # DISCUSSION

401 Our previous work in the young TG^{AC8} heart, a model of increased chronic cardiac
402 workload by sustained activation of the AC/cAMP/PKA/Ca^{2+} axis, has shown that several
403 adaptation mechanisms protect the TG^{AC8} heart health and function[16]. Among other
404 mechanisms, protein quality control, including the UPS and the autophagic machinery,
405 were upregulated, and had a key role in ensuring health heart structure and function. The
406 present study evaluated proteostasis in detail focusing on key players involved in the
407 autophagic process and revealed that in a context of lifetime exposure (up to 18-21 to
408 months) to chronic cardiac cAMP-induced stress, PQC mechanisms fail more severely.

409 In toto, our results demonstrate that the young TG^{AC8} heart upregulates the autophagy
410 process by fine tuning key effectors, such as LC3, in their localization and isoforms (A
411 and B), which localize to different phagophores/autophagosomes[40], suggesting isotype-
412 specific functions that guarantee effective clearance of damaged proteins in a scenario
413 of high cardiac workload.

414 Specifically, at 3 months of age, both LC3**AI** (the cytosolic form of LC3, which
415 becomes lipidated to LC3II) and LC3**BII** (the lipidated LC3I, which localizes on
416 autophagosomes and autophagolysosomes[41] during autophagy), differed in TG^{AC8} vs
417 WT, in a scenario indicative of upregulated autophagy. LC3**AI** upregulation was both
418 transcriptional[16] and translational, and since LC3A, together with FKBP8, also
419 upregulated in TG^{AC8}, are important markers of mitophagy, we speculate upregulation of
420 both LC3A and FKBP8 important for PQC in the TG^{AC8} heart. Moreover, because LC3
421 isoforms are present on different autophagosomes, suggesting different functions[40], the
422 significant LC3**BII** downregulation in TG^{AC8} vs age-matched WT, confirms the possible
423 involvement of LC3A and LC3B in different signaling pathways (mitophagy[42,43] vs
424 apoptosis[44] vs endosome-mediated autophagy[45,46]). LC3 post-translational modifications
425 (PTMs) by phosphorylation, which affect its activity[27,28], were also differently modulated
426 in the young TG^{AC8} vs WT heart favoring both early and late autophagy stages:
427 specifically, LC3-S12 was significantly downregulated, whereas LC3-T50 was
428 significantly upregulated. Phosphorylation at S12 by PKA/PKC[47] inhibits autophagy, by
429 preventing autophagosome wall elongation, whereas phosphorylation at T50 by STK3/4[28]
430 is stimulatory for the autophagic process, by promoting autophagolysosome fusion.

431 Sequestosome-1, also known as p62[48], an essential autophagy adaptor that
432 colocalizes with ubiquitin and LC3, was also significantly upregulated in the young TG^{AC8}
433 heart. p62 plays a critical and protective role in “aggresome” formation and autophagic
434 activation by recognizing cargo tagged for disposal and transporting it to the
435 lysosome[49,50], while itself being an autophagy substrate[51]. Phospho-forms p62-S403,
436 p62-S349, and the ratios of phosphorylated p62 to total p62, were upregulated in TG^{AC8}
437 vs WT at 3 months. Specifically, p62 phosphorylation at S403, which increases its
438 selectivity and affinity towards ubiquitin, has been shown to positively correlate to
439 ubiquitinated cargo[52], including protein aggregates[53] and polyubitiquinated
440 mitochondria[52]; p62 phosphorylation at S349, in contrast, has a higher affinity for the
441 ubiquitin ligase adaptor Kelch-like ECH-associated protein 1 (KEAP1)[54], resulting in
442 constitutive activation of the transcription factor NF-E2-related factor 2 (NRF2) and
443 regulation of its downstream signaling pathways[55]. Upregulation of p62 and it phospho-
444 forms in the young TG^{AC8} heart demonstrates its adaptation to the sequelae of sustained
445 activation of the AC/cAMP/PKA/Ca^{2+} axis, involving both upregulation of signaling for
446 “aggresome” clearance and increased ROS scavenging, a protection mechanism from
447 oxidative stress by the increased cardiac workload.

448 Autophagy flux was increased in TG^{AC8} vs WT at 3 months. Specifically, the flux of
449 LC3 and p62 markers was accelerated, as shown by the increased LC3II/LC3I ratios
450 following CQ treatment, because of accumulation of LC3II at the lysosome. In addition,
451 cathepsin L1 activity was upregulated in TG^{AC8}, and protein levels of the lysosomal acid
452 phosphatase ACP2 were also increased in TG^{AC8}, which together with the results of our
453 previous study showing increased proteasome activity without accumulation of insoluble

454 protein aggregates, and increased levels of proteins involved in the autophagic
455 machinery[16], confirm that UPS and autophagic pathways concurrently operate in the
456 young TG^{AC8} heart to manage its chronic cardiac cAMP-derived stress[56,57].

457 With aging, autophagy markers LC3 and the autophagy related 4B cysteine peptidase
458 (ATG4B), involved in LC3 lifecycle[29], became significantly downregulated in both TG^{AC8}
459 and WT, with no difference, indicating that cardiac aging per se, impacts negatively on
460 PQC. However, assessment of autophagy flux revealed that flux of LC3A and p62 was
461 *upregulated* in old TG^{AC8}, compared to age-matched WT, in a context of a reduced overall
462 autophagic flux, as demonstrated by reduced numbers of early autophagy figures, and
463 an increased number of late autophagic events (by TEM quantification).

464 Accelerated autophagy marker flux, however, has been shown to be a compensating
465 mechanism contributing to the remodeling of the myocardium under stress[58], which can
466 be maladaptive in disease conditions. We interpret the higher p62 flux within the context
467 of chronic upregulation of the AC/cAMP/PKA/Ca^{2+} axis, as a sensing mechanism for the
468 increased presence of aggresomes which, if not cleared, need compartmentalization.
469 Moreover, a faster LC3A flux may indicate increased mitochondria tagged for disposal,
470 an index of garbage production/accumulation.

471 Although mitochondria carry out several critical and diverse functions[56], a steady
472 production and supply of adenosine triphosphate (ATP) via oxidative phosphorylation is
473 absolutely required by the heart, because of its continuous high demand for energy, and
474 this is why cardiomyocytes have extremely high mitochondrial density. However, it is
475 established that mitochondria and lysosomes of long-lived cells such as cardiac myocytes
476 suffer remarkable age-related alterations as the cellular turnover machinery becomes

477 inherently imperfect[59] with age. Mitochondrial changes, by continuous physiological
478 oxidative stress[59] and increased reactive oxygen species (ROS) production, include
479 structural disorganization and enlargement, while lysosomes, which are responsible for
480 autophagic turnover of mitochondria, accumulate LF (age pigment), a polymeric,
481 autofluorescent, undegradable material, mainly composed of proteins and lipids[60]. When
482 mitochondria become damaged and/or dysfunctional[2,57], unable to support the high
483 energy demands, and overall mitochondrial fitness declines, heart function deteriorates
484 leading to disease conditions.

485 The cooperation of LC3A with the non-canonical mitophagy receptor FKBP8,
486 assigning a new important role in mitophagy to LC3A and the process of mitochondrial
487 turnover, renders LC3A an important informant of mitochondrial fitness, in the adult
488 cardiac tissue[42]. In old TG^{AC8}, all mitophagy pathways were activated, compared to age-
489 matched WT controls. However, a faster LC3A flux together with upregulated mitophagy
490 signaling through a variety of pathways[61], suggests a failing mitophagy and poor
491 mitochondrial fitness/function, possibly due to insufficient lysosomal activity.

492 Mitochondrial structure (assessed by semi-thin stain by TEM) was severely damaged
493 in old TG^{AC8}, showing a significant, and more aberrant accumulation of LF bodies with
494 increased size, and a distribution covering a higher percentage of cardiomyocyte area.
495 LF aggregates are not removed from the cytosol by the UPS[62], because they are
496 covalently cross-linked aggregates, and their accumulation at the later stage of autophagy
497 is an indication of lysosomal impairment[63], which, together with their known accumulation
498 with advancing age, suggests that the old TG^{AC8} portrays a phenotype of accelerated
499 cardiac aging, compared to age-matched WT. In addition, the brown to black pigment

500 aggregates, in the old TG^{AC8} but not in age-matched WT suggests changes in cargo
501 processing, with accumulation of specific material.

502 In addition to failure at the lysosome, changes in UPS activity and expression,
503 reflecting metabolic, functional, or simply structural changes in response to the different
504 demands for the turnover of signaling and structural proteins, accompany aging.
505 Specifically in the heart, proteasomal insufficiency has been linked to accumulation of
506 protein aggregates, whereas alterations of structural proteins, such as disorganization of
507 desmin filaments, which interlink the contractile myofibrillar apparatus with mitochondria,
508 nuclei and the sarcolemma, has been shown to affect mitochondrial positioning, therefore
509 compromising mitochondrial function, and leading to cardiomyocyte dysfunction[38,64].
510 Because the negative modulation of desmin's physical properties and assembly by its
511 PTMs, leads to the build-up of cardiac preamiloyd oligomers (PAOs) and has been
512 recently indicated to be an index of premature and acquired heart failure (as occurred in
513 TG^{AC8} at 18 months), we evaluated desmin structure, and quantified accumulation of
514 cardiac PAOs, in old TG^{AC8}. Results showed that desmin was significantly tagged for
515 ubiquitination and cleaved in old TG^{AC8} heart, compared to age-matched WT, and that
516 PAOs accumulation was also highly increased.

517 Although translation rates did not differ between genotypes at an old age, protein
518 synthesis significantly decreased with aging in TG^{AC8} heart at 19-months compared to 3-
519 months, in line with the normal aging process[30,31], indicating that the TG^{AC8} heart
520 optimizes energy use with age, by decreasing the formation of *de-novo* proteins in order
521 to focus on repairing the existing proteome, a mechanism that preserves and increases,
522 life span[32].

523 However, protein aggregates significantly accumulated in the old TG^{AC8} heart
524 compared to age-matched WT. This scenario suggests an increased ubiquitination
525 signaling within a context of proteasomal insufficiency which, together with a faster
526 autophagy flux, indicate maladaptive responses with ineffective cargo clearance
527 demonstrated in hearts or cardiomyocytes under disease and pathological conditions[65],
528 including desminopathy[58].

529 Therefore, this study demonstrates that severe loss of proteostasis is due to loss of
530 PQC in the old TG^{AC8} heart, compared to age-matched WT.

531 In conclusion, chronic cardiac AC-dependent cAMP-stress, although activating
532 protective signaling circuitry that preserve heart health early in life, accelerates cardiac
533 aging and reduces cardiac health span, resulting in cardiomyopathy[17].

534

535 ## ACKNOWLEDGMENTS

536 The study was designed by M.G.P. and E.G.L. The experiments were conducted by
537 M.G.P., M.C.B., G.A., M.R., D.R.R., and K.C. The data were analyzed by M.G.P., M.C.B.,
538 G.A., M.R., C.H.M., and J.Q. The article was written by M.G.P. and E.G.L., and approved
539 by all authors.

540 ## SOURCES OF FUNDING

541 This research was supported entirely by the Intramural Research Program of the NIH,
542 National Institute on Aging (USA).

543 ## DISCLOSURES

544 None.

545 ## REFERENCES

546 1. Taylor RC, Dillin A. Aging as an event of proteostasis collapse. *Cold Spring Harb Perspect Biol*.
547 2011;3. doi: 10.1101/cshperspect.a004440
548 2. Linton PJ, Gurney M, Sengstock D, Mentzer RM, Jr., Gottlieb RA. This old heart: Cardiac aging and
549 autophagy. *J Mol Cell Cardiol*. 2015;83:44-54. doi: 10.1016/j.yjmcc.2014.12.017
550 3. Kholova I, Niessen HW. Amyloid in the cardiovascular system: a review. *J Clin Pathol*. 2005;58:125-
551 133. doi: 10.1136/jcp.2004.017293
552 4. Agnetti G, Halperin VL, Kirk JA, Chakir K, Guo Y, Lund L, Nicolini F, Gherli T, Guarnieri C, Caldarera
553 CM, et al. Desmin modifications associate with amyloid-like oligomers deposition in heart failure.
554 *Cardiovasc Res*. 2014;102:24-34. doi: 10.1093/cvr/cvu003
555 5. Sanbe A, Osinska H, Saffitz JE, Glabe CG, Kayed R, Maloyan A, Robbins J. Desmin-related
556 cardiomyopathy in transgenic mice: a cardiac amyloidosis. *Proc Natl Acad Sci U S A*.
557 2004;101:10132-10136. doi: 10.1073/pnas.0401900101
558 6. Del Monte F, Agnetti G. Protein post-translational modifications and misfolding: new concepts in
559 heart failure. *Proteomics Clin Appl*. 2014;8:534-542. doi: 10.1002/prca.201400037
560 7. Rainer PP, Dong P, Sorge M, Fert-Bober J, Holewinski RJ, Wang Y, Foss CA, An SS, Baracca A, Solaini
561 G, et al. Desmin Phosphorylation Triggers Preamyloid Oligomers Formation and Myocyte
562 Dysfunction in Acquired Heart Failure. *Circ Res*. 2018;122:e75-e83. doi:
563 10.1161/CIRCRESAHA.117.312082
564 8. Mizushima N, Levine B, Cuervo AM, Klionsky DJ. Autophagy fights disease through cellular self-
565 digestion. *Nature*. 2008;451:1069-1075. doi: 10.1038/nature06639
566 9. Wilhelm T, Richly H. Autophagy during ageing - from Dr Jekyll to Mr Hyde. *FEBS J*. 2018;285:2367-
567 2376. doi: 10.1111/febs.14453

568 10. Marzabadi MR, Sohal RS, Brunk UT. Mechanisms of lipofuscinogenesis: effect of the inhibition of
569 lysosomal proteinases and lipases under varying concentrations of ambient oxygen in cultured rat
570 neonatal myocardial cells. *APMIS*. 1991;99:416-426. doi: 10.1111/j.1699-0463.1991.tb05170.x
571 11. Lopez-Otin C, Blasco MA, Partridge L, Serrano M, Kroemer G. Hallmarks of aging: An expanding
572 universe. *Cell*. 2023;186:243-278. doi: 10.1016/j.cell.2022.11.001
573 12. Munnell JF, Getty R. Rate of accumulation of cardiac lipofuscin in the aging canine. *J Gerontol*.
574 1968;23:154-158. doi: 10.1093/geronj/23.2.154
575 13. Nakano M, Oenzil F, Mizuno T, Gotoh S. Age-related changes in the lipofuscin accumulation of
576 brain and heart. *Gerontology*. 1995;41 Suppl 2:69-79. doi: 10.1159/000213726
577 14. Moen JM, Matt MG, Ramirez C, Tarasov KV, Chakir K, Tarasova YS, Lukyanenko Y, Tsutsui K,
578 Monfredi O, Morrell CH, et al. Overexpression of a Neuronal Type Adenylyl Cyclase (Type 8) in
579 Sinoatrial Node Markedly Impacts Heart Rate and Rhythm. *Front Neurosci*. 2019;13:615. doi:
580 10.3389/fnins.2019.00615
581 15. Zhang X, Szeto C, Gao E, Tang M, Jin J, Fu Q, Makarewich C, Ai X, Li Y, Tang A, et al. Cardiotoxic
582 and cardioprotective features of chronic beta-adrenergic signaling. *Circ Res*. 2013;112:498-509.
583 doi: 10.1161/CIRCRESAHA.112.273896
584 16. Tarasov KV, Chakir K, Riordon DR, Lyashkov AE, Ahmet I, Perino MG, Silvester AJ, Zhang J, Wang
585 M, Lukyanenko YO, et al. A remarkable adaptive paradigm of heart performance and protection
586 emerges in response to marked cardiac-specific overexpression of ADCY8. *Elife*. 2022;11. doi:
587 10.7554/eLife.80949
588 17. Lipskaia L, Defer N, Esposito G, Hajar I, Garel MC, Rockman HA, Hanoune J. Enhanced cardiac
589 function in transgenic mice expressing a Ca(2+)-stimulated adenylyl cyclase. *Circ Res*.
590 2000;86:795-801. doi: 10.1161/01.res.86.7.795
591 18. Georget M, Mateo P, Vandecasteele G, Jurevicius J, Lipskaia L, Defer N, Hanoune J, Hoerter J,
592 Fischmeister R. Augmentation of cardiac contractility with no change in L-type Ca2+ current in
593 transgenic mice with a cardiac-directed expression of the human adenylyl cyclase type 8 (AC8).
594 *FASEB J*. 2002;16:1636-1638. doi: 10.1096/fj.02-0292fje
595 19. Georget M, Mateo P, Vandecasteele G, Lipskaia L, Defer N, Hanoune J, Hoerter J, Lugnier C,
596 Fischmeister R. Cyclic AMP compartmentation due to increased cAMP-phosphodiesterase activity
597 in transgenic mice with a cardiac-directed expression of the human adenylyl cyclase type 8 (AC8).
598 *FASEB J*. 2003;17:1380-1391. doi: 10.1096/fj.02-0784com
599 20. Mougenot N, Mika D, Czibik G, Marcos E, Abid S, Houssaini A, Vallin B, Guellich A, Mehel H, Sawaki
600 D, et al. Cardiac adenylyl cyclase overexpression precipitates and aggravates age-related
601 myocardial dysfunction. *Cardiovasc Res*. 2019;115:1778-1790. doi: 10.1093/cvr/cvy306
602 21. Liu Y, Zhou K, Li J, Agvanian S, Caldaruse AM, Shaw S, Hitzeman TC, Shaw RM, Hong T. In Mice
603 Subjected to Chronic Stress, Exogenous cBIN1 Preserves Calcium-Handling Machinery and Cardiac
604 Function. *JACC Basic Transl Sci*. 2020;5:561-578. doi: 10.1016/j.jacbts.2020.03.006
605 22. Zhang GX, Kimura S, Nishiyama A, Shokoji T, Rahman M, Yao L, Nagai Y, Fujisawa Y, Miyatake A,
606 Abe Y. Cardiac oxidative stress in acute and chronic isoproterenol-infused rats. *Cardiovasc Res*.
607 2005;65:230-238. doi: 10.1016/j.cardiores.2004.08.013
608 23. Weibel ER. *Stereological methods*. London ; New York: Academic Press; 1979.
609 24. Palade GE. A study of fixation for electron microscopy. *J Exp Med*. 1952;95:285-298. doi:
610 10.1084/jem.95.3.285
611 25. Kayed R, Head E, Thompson JL, McIntire TM, Milton SC, Cotman CW, Glabe CG. Common structure
612 of soluble amyloid oligomers implies common mechanism of pathogenesis. *Science*.
613 2003;300:486-489. doi: 10.1126/science.1079469
614 26. Ferreira JA, Zwinderman AH. On the Benjamini-Hochberg method. *Ann Stat*. 2006;34:1827-1849.
615 doi: 10.1214/009053606000000425

616 27. Cherra SJ, 3rd, Kulich SM, Uechi G, Balasubramani M, Mountzouris J, Day BW, Chu CT. Regulation
617 of the autophagy protein LC3 by phosphorylation. *J Cell Biol*. 2010;190:533-539. doi:
618 10.1083/jcb.201002108
619 28. Wilkinson DS, Jariwala JS, Anderson E, Mitra K, Meisenhelder J, Chang JT, Ideker T, Hunter T, Nizet
620 V, Dillin A, et al. Phosphorylation of LC3 by the Hippo kinases STK3/STK4 is essential for autophagy.
621 *Mol Cell*. 2015;57:55-68. doi: 10.1016/j.molcel.2014.11.019
622 29. Scherz-Shouval R, Shvets E, Fass E, Shorer H, Gil L, Elazar Z. Reactive oxygen species are essential
623 for autophagy and specifically regulate the activity of Atg4. *EMBO J*. 2007;26:1749-1760. doi:
624 10.1038/sj.emboj.7601623
625 30. Anisimova AS, Alexandrov AI, Makarova NE, Gladyshev VN, Dmitriev SE. Protein synthesis and
626 quality control in aging. *Aging (Albany NY)*. 2018;10:4269-4288. doi: 10.18632/aging.101721
627 31. Anisimova AS, Meerson MB, Gerashchenko MV, Kulakovskiy IV, Dmitriev SE, Gladyshev VN.
628 Multifaceted deregulation of gene expression and protein synthesis with age. *Proc Natl Acad Sci*
629 *U S A*. 2020;117:15581-15590. doi: 10.1073/pnas.2001788117
630 32. Hipkiss AR. On why decreasing protein synthesis can increase lifespan. *Mech Ageing Dev*.
631 2007;128:412-414. doi: 10.1016/j.mad.2007.03.002
632 33. Moyzis A, Gustafsson AB. Multiple recycling routes: Canonical vs. non-canonical mitophagy in the
633 heart. *Biochim Biophys Acta Mol Basis Dis*. 2019;1865:797-809. doi: 10.1016/j.bbadis.2018.09.034
634 34. Narendra D, Tanaka A, Suen DF, Youle RJ. Parkin is recruited selectively to impaired mitochondria
635 and promotes their autophagy. *J Cell Biol*. 2008;183:795-803. doi: 10.1083/jcb.200809125
636 35. Matsumoto G, Shimogori T, Hattori N, Nukina N. TBK1 controls autophagosomal engulfment of
637 polyubiquitinated mitochondria through p62/SQSTM1 phosphorylation. *Hum Mol Genet*.
638 2015;24:4429-4442. doi: 10.1093/hmg/ddv179
639 36. Jain A, Lamark T, Sjottem E, Larsen KB, Awuh JA, Overvatn A, McMahon M, Hayes JD, Johansen T.
640 p62/SQSTM1 is a target gene for transcription factor NRF2 and creates a positive feedback loop
641 by inducing antioxidant response element-driven gene transcription. *J Biol Chem*.
642 2010;285:22576-22591. doi: 10.1074/jbc.M110.118976
643 37. Misaka T, Murakawa T, Nishida K, Omori Y, Taneike M, Omiya S, Molenaar C, Uno Y, Yamaguchi
644 O, Takeda J, et al. FKBP8 protects the heart from hemodynamic stress by preventing the
645 accumulation of misfolded proteins and endoplasmic reticulum-associated apoptosis in mice. *J*
646 *Mol Cell Cardiol*. 2018;114:93-104. doi: 10.1016/j.yjmcc.2017.11.004
647 38. Alam S, Abdullah CS, Aishwarya R, Miriyala S, Panchatcharam M, Peretik JM, Orr AW, James J,
648 Robbins J, Bhuiyan MS. Aberrant Mitochondrial Fission Is Maladaptive in Desmin Mutation-
649 Induced Cardiac Proteotoxicity. *J Am Heart Assoc*. 2018;7. doi: 10.1161/JAHA.118.009289
650 39. Agnetti G, Herrmann H, Cohen S. New roles for desmin in the maintenance of muscle homeostasis.
651 *FEBS J*. 2022;289:2755-2770. doi: 10.1111/febs.15864
652 40. Koukourakis MI, Kalamida D, Giatromanolaki A, Zois CE, Sivridis E, Pouliliou S, Mitrakas A, Gatter
653 KC, Harris AL. Autophagosome Proteins LC3A, LC3B and LC3C Have Distinct Subcellular
654 Distribution Kinetics and Expression in Cancer Cell Lines. *PLoS One*. 2015;10:e0137675. doi:
655 10.1371/journal.pone.0137675
656 41. Tanida I, Minematsu-Ikeguchi N, Ueno T, Kominami E. Lysosomal turnover, but not a cellular level,
657 of endogenous LC3 is a marker for autophagy. *Autophagy*. 2005;1:84-91. doi:
658 10.4161/auto.1.2.1697
659 42. Bhujabal Z, Birgisdottir AB, Sjottem E, Brenne HB, Overvatn A, Habisov S, Kirkin V, Lamark T,
660 Johansen T. FKBP8 recruits LC3A to mediate Parkin-independent mitophagy. *EMBO Rep*.
661 2017;18:947-961. doi: 10.15252/embr.201643147

662 43. Chu CT, Bayir H, Kagan VE. LC3 binds externalized cardiolipin on injured mitochondria to signal
663 mitophagy in neurons: implications for Parkinson disease. *Autophagy*. 2014;10:376-378. doi:
664 10.4161/auto.27191
665 44. Satyavarapu EM, Das R, Mandal C, Mukhopadhyay A, Mandal C. Autophagy-independent
666 induction of LC3B through oxidative stress reveals its non-canonical role in anoikis of ovarian
667 cancer cells. *Cell Death Dis*. 2018;9:934. doi: 10.1038/s41419-018-0989-8
668 45. Kondylis V, van Nispen Tot Pannerden HE, van Dijk S, Ten Broeke T, Wubbolts R, Geerts WJ, Seinen
669 C, Mutis T, Heijnen HF. Endosome-mediated autophagy: an unconventional MIIC-driven
670 autophagic pathway operational in dendritic cells. *Autophagy*. 2013;9:861-880. doi:
671 10.4161/auto.24111
672 46. Magne J, Green DR. LC3-associated endocytosis and the functions of Rubicon and ATG16L1. *Sci*
673 *Adv*. 2022;8:eabo5600. doi: 10.1126/sciadv.abo5600
674 47. Jiang H, Cheng D, Liu W, Peng J, Feng J. Protein kinase C inhibits autophagy and phosphorylates
675 LC3. *Biochem Biophys Res Commun*. 2010;395:471-476. doi: 10.1016/j.bbrc.2010.04.030
676 48. Rusten TE, Stenmark H. p62, an autophagy hero or culprit? *Nat Cell Biol*. 2010;12:207-209. doi:
677 10.1038/ncb0310-207
678 49. Lamark T, Svenning S, Johansen T. Regulation of selective autophagy: the p62/SQSTM1 paradigm.
679 *Essays Biochem*. 2017;61:609-624. doi: 10.1042/EBC20170035
680 50. Johansen T, Lamark T. Selective autophagy mediated by autophagic adapter proteins. *Autophagy*.
681 2011;7:279-296. doi: 10.4161/auto.7.3.14487
682 51. Bjorkoy G, Lamark T, Brech A, Outzen H, Perander M, Overvatn A, Stenmark H, Johansen T.
683 p62/SQSTM1 forms protein aggregates degraded by autophagy and has a protective effect on
684 huntingtin-induced cell death. *J Cell Biol*. 2005;171:603-614. doi: 10.1083/jcb.200507002
685 52. Matsumoto G, Wada K, Okuno M, Kurosawa M, Nukina N. Serine 403 phosphorylation of
686 p62/SQSTM1 regulates selective autophagic clearance of ubiquitinated proteins. *Mol Cell*.
687 2011;44:279-289. doi: 10.1016/j.molcel.2011.07.039
688 53. Lim J, Lachenmayer ML, Wu S, Liu W, Kundu M, Wang R, Komatsu M, Oh YJ, Zhao Y, Yue Z.
689 Proteotoxic stress induces phosphorylation of p62/SQSTM1 by ULK1 to regulate selective
690 autophagic clearance of protein aggregates. *PLoS Genet*. 2015;11:e1004987. doi:
691 10.1371/journal.pgen.1004987
692 54. Ichimura Y, Waguri S, Sou YS, Kageyama S, Hasegawa J, Ishimura R, Saito T, Yang Y, Kouno T,
693 Fukutomi T, et al. Phosphorylation of p62 activates the Keap1-Nrf2 pathway during selective
694 autophagy. *Mol Cell*. 2013;51:618-631. doi: 10.1016/j.molcel.2013.08.003
695 55. Jiang T, Harder B, Rojo de la Vega M, Wong PK, Chapman E, Zhang DD. p62 links autophagy and
696 Nrf2 signaling. *Free Radic Biol Med*. 2015;88:199-204. doi: 10.1016/j.freeradbiomed.2015.06.014
697 56. McBride HM, Neuspiel M, Wasiak S. Mitochondria: more than just a powerhouse. *Curr Biol*.
698 2006;16:R551-560. doi: 10.1016/j.cub.2006.06.054
699 57. Gottlieb RA, Carreira RS. Autophagy in health and disease. 5. Mitophagy as a way of life. *Am J*
700 *Physiol Cell Physiol*. 2010;299:C203-210. doi: 10.1152/ajpcell.00097.2010
701 58. Zheng Q, Su H, Ranek MJ, Wang X. Autophagy and p62 in cardiac proteinopathy. *Circ Res*.
702 2011;109:296-308. doi: 10.1161/CIRCRESAHA.111.244707
703 59. Terman A, Brunk UT. The aging myocardium: roles of mitochondrial damage and lysosomal
704 degradation. *Heart Lung Circ*. 2005;14:107-114. doi: 10.1016/j.hlc.2004.12.023
705 60. Konig J, Ott C, Hugo M, Jung T, Bulteau AL, Grune T, Hohn A. Mitochondrial contribution to
706 lipofuscin formation. *Redox Biol*. 2017;11:673-681. doi: 10.1016/j.redox.2017.01.017
707 61. Moyzis AG, Sadoshima J, Gustafsson AB. Mending a broken heart: the role of mitophagy in
708 cardioprotection. *Am J Physiol Heart Circ Physiol*. 2015;308:H183-192. doi:
709 10.1152/ajpheart.00708.2014

62. Hohn A, Jung T, Grimm S, Catalgol B, Weber D, Grune T. Lipofuscin inhibits the proteasome by binding to surface motifs. *Free Radic Biol Med*. 2011;50:585-591. doi: 10.1016/j.freeradbiomed.2010.12.011
63. Hohn A, Sittig A, Jung T, Grimm S, Grune T. Lipofuscin is formed independently of macroautophagy and lysosomal activity in stress-induced prematurely senescent human fibroblasts. *Free Radic Biol Med*. 2012;53:1760-1769. doi: 10.1016/j.freeradbiomed.2012.08.591
64. Bar H, Strelkov SV, Sjoberg G, Aebi U, Herrmann H. The biology of desmin filaments: how do mutations affect their structure, assembly, and organisation? *J Struct Biol*. 2004;148:137-152. doi: 10.1016/j.jsb.2004.04.003
65. Day SM. The ubiquitin proteasome system in human cardiomyopathies and heart failure. *Am J Physiol Heart Circ Physiol*. 2013;304:H1283-1293. doi: 10.1152/ajpheart.00249.2012

MIN NUMBER SEEN in papers is #46

MAX NUMBER SEEN in papers is #70

725 ## GRAPHIC ABSTRACT

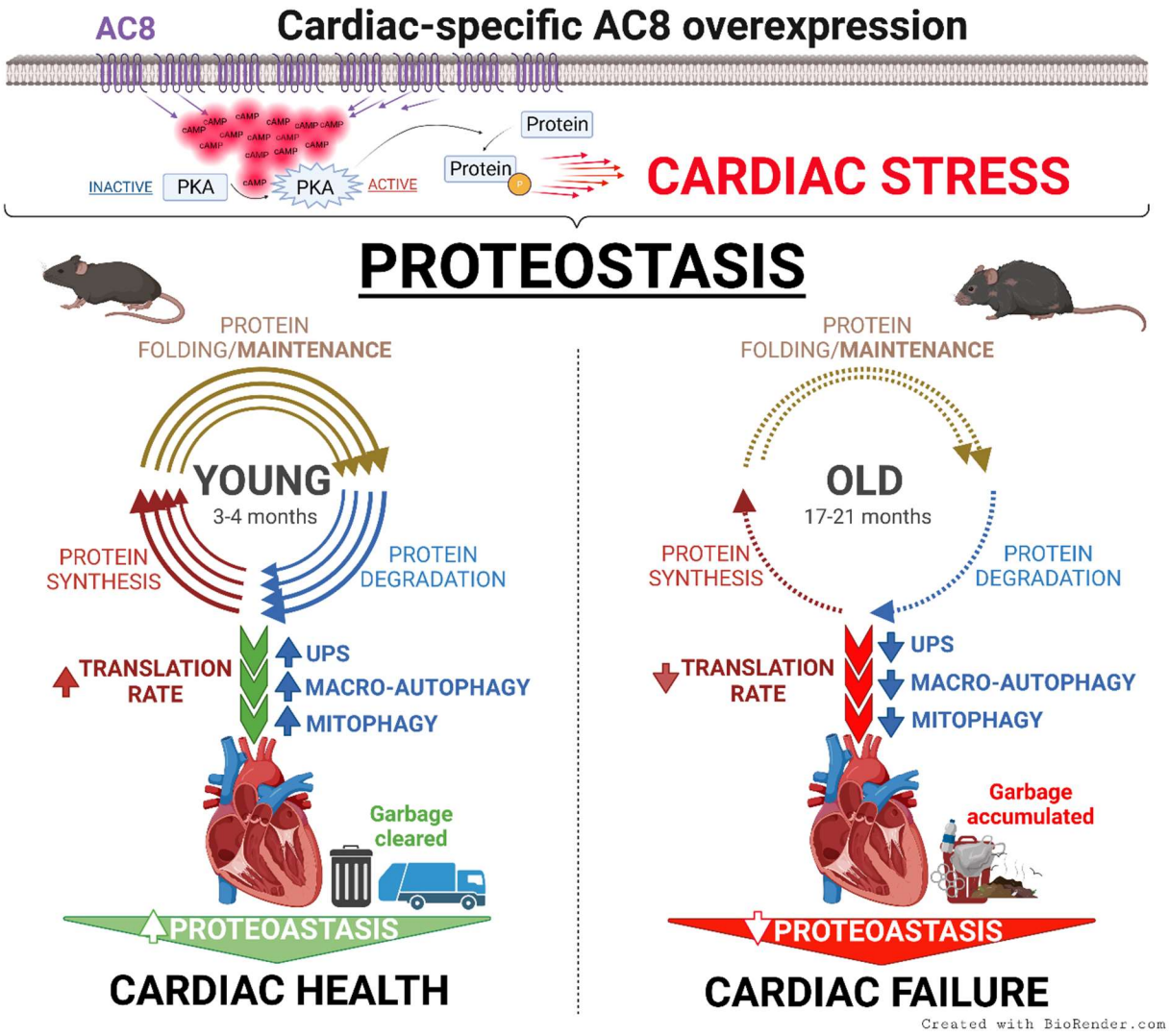

726

727 **Table. Proteostasis in young and aged TG^{AC8} in the context of cardiac stress**
728 **following cardiac-specific constitutive stimulation of the AC/cAMP/PKA/Ca^{2+} axis**
729 **by α-MHC-driven AC8 overexpression.**

FIGURES WITH FIGURE LEGENDS

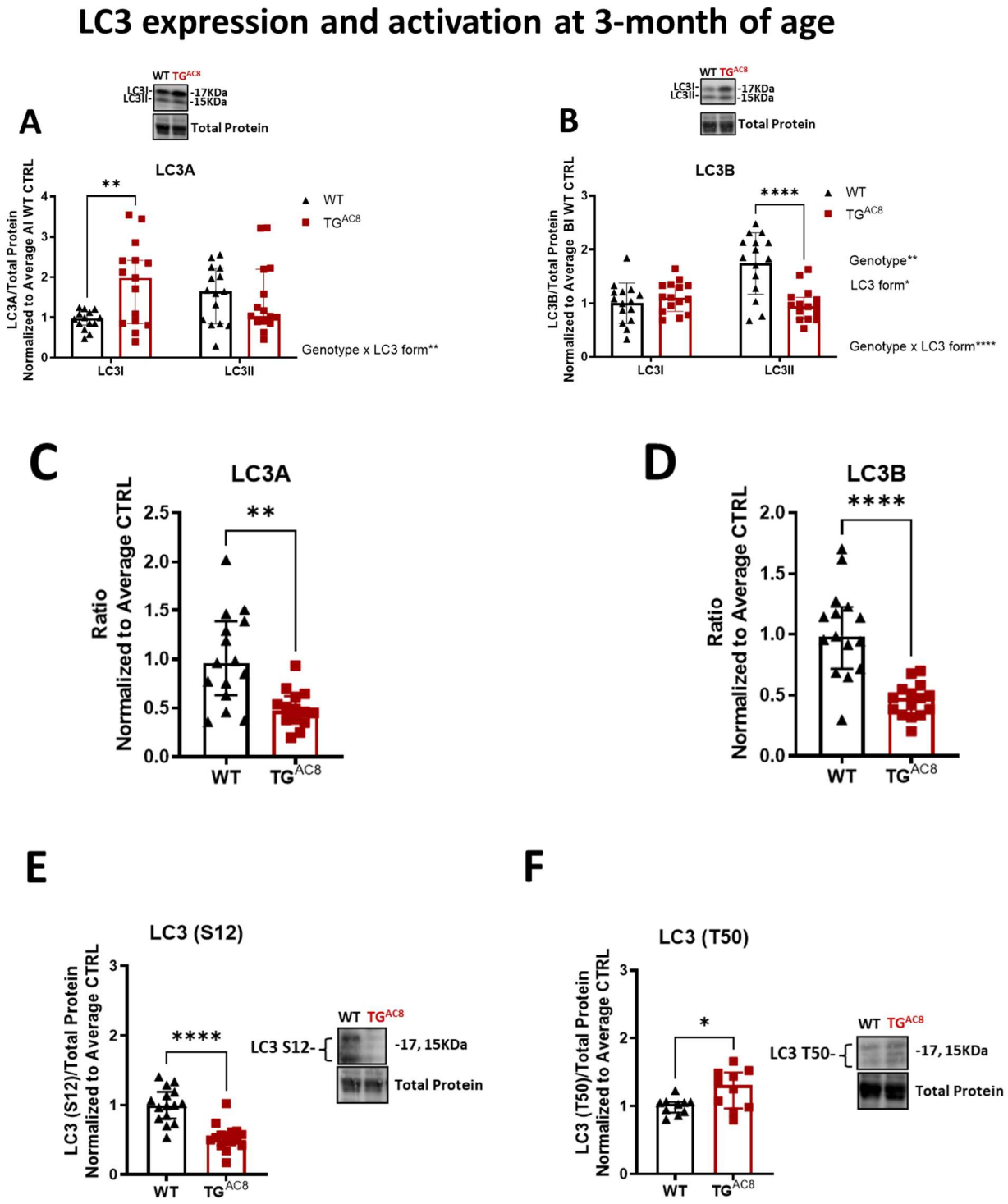

Figure 1. At 3-month of age LC3 isoforms are differently modulated in TG^{AC8}, and autophagy is promoted.

736 Bar graphs and Western blot analysis of the autophagy marker LC3, LC3II/LC3I ratios,
737 and LC3 phosphorylation in young TG^{AC8} LV and wild type (WT) at 3 months of age (n=15
738 mice per group). Data are presented as the median ± interquartile range **A**), LC3A; **B**),
739 LC3B; **C**), LC3AII/LC3AI; **D**), LC3BII/LC3BI; **E**), LC3-S12; **F**), LC3-T50. **A and B**, A mixed-
740 effect model for repeated measurements, followed by Original FDR method of Benjamini
741 and Hochberg post-hoc multi-comparison test was used. **C, D, E and F**, Unpaired 2-tailed
742 Students tests with Welch's correction was used.

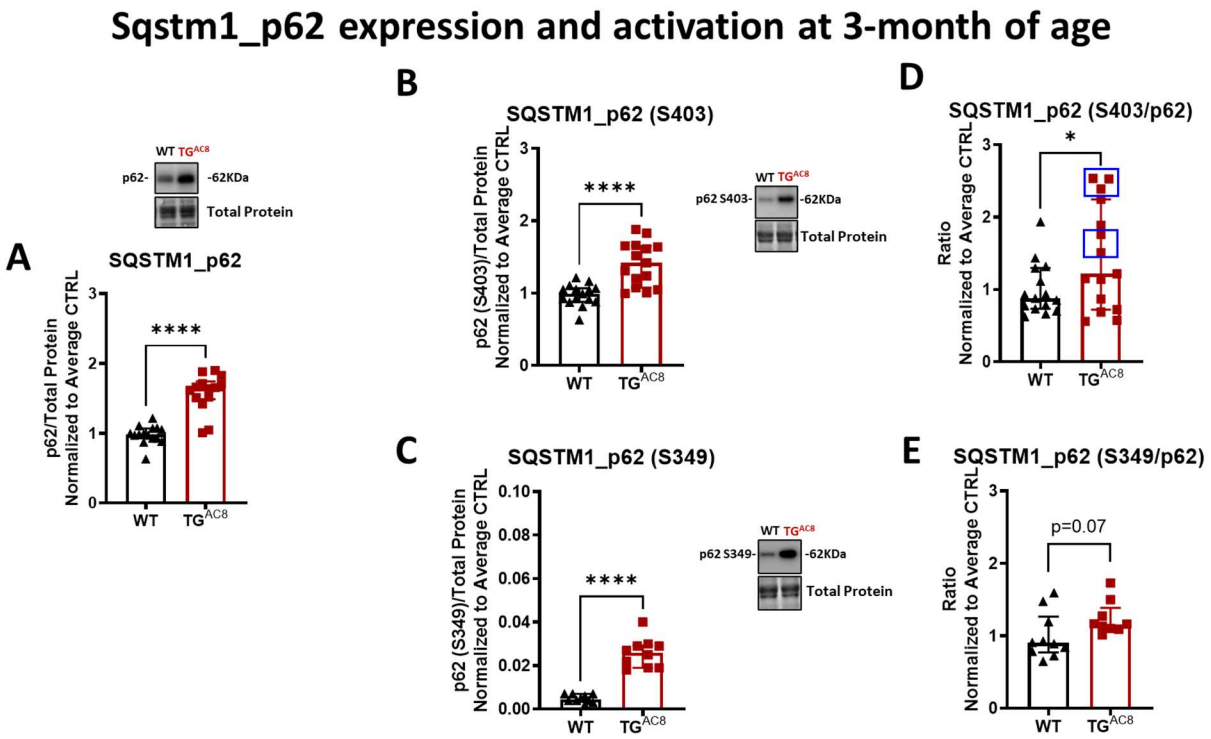

743

744 **Figure 2. Sqstm1_p62 expression and phosphorylation are increased in TG^{AC8} at 3-**
745 **month of age.**

746 Bar graphs and Western blot analysis of the autophagy cargo receptor p62, its post-
747 translational modifications, and their ratios to total p62 in TG^{AC8} and WT at 3 months of
748 age (n=15 mice per group). **A**), Total p62; **B**), p62-S403; **C**), p62-S349; **D**), p62-S403/p62;

749 **E**), p62-S349/p62. Unpaired 2-tailed Student t test with Welch's correction was used and

750 data are presented as the median ± interquartile range.

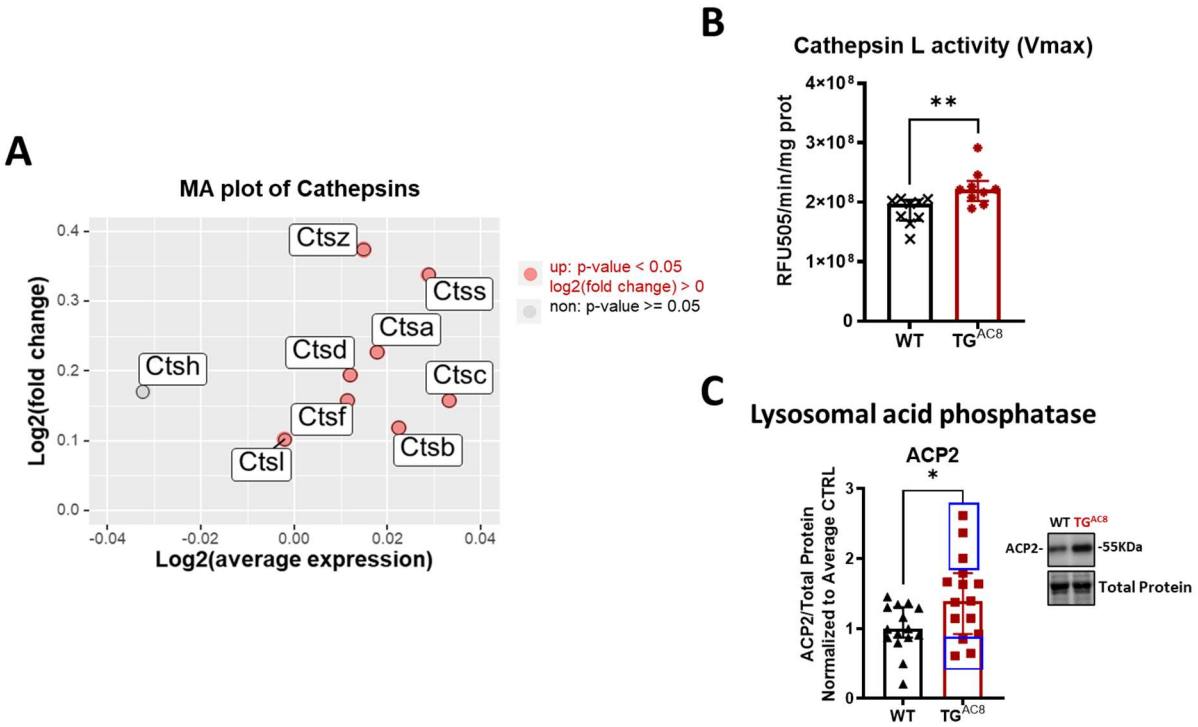

751

752 **Figure 3. Lysosome performance is higher in young TG^{AC8}.**

753 **A**), MA plot showing enrichment in the relative amount of lysosomal cathepsin obtained

754 from OMICs data in TG^{AC8} at 3 months of age. **B**), Cathepsin L1 activity measured in

755 TG^{AC8} and WT littermate at 3 months of age (n=6 mice per group). Activity was measured

756 at V_{max}, and it is plotted as emitted fluorescence per mL, per mg of protein. **C**), Bar graphs

757 and Western blot analysis of the lysosomal acid phosphatase, ACP2 (n=15 mice per

758 group). Unpaired 2-tailed Student t test was used in **B** and unpaired 2-tailed Student t test

759 with Welch's correction was used in **C**. Data are presented as the median ± interquartile

760 range.

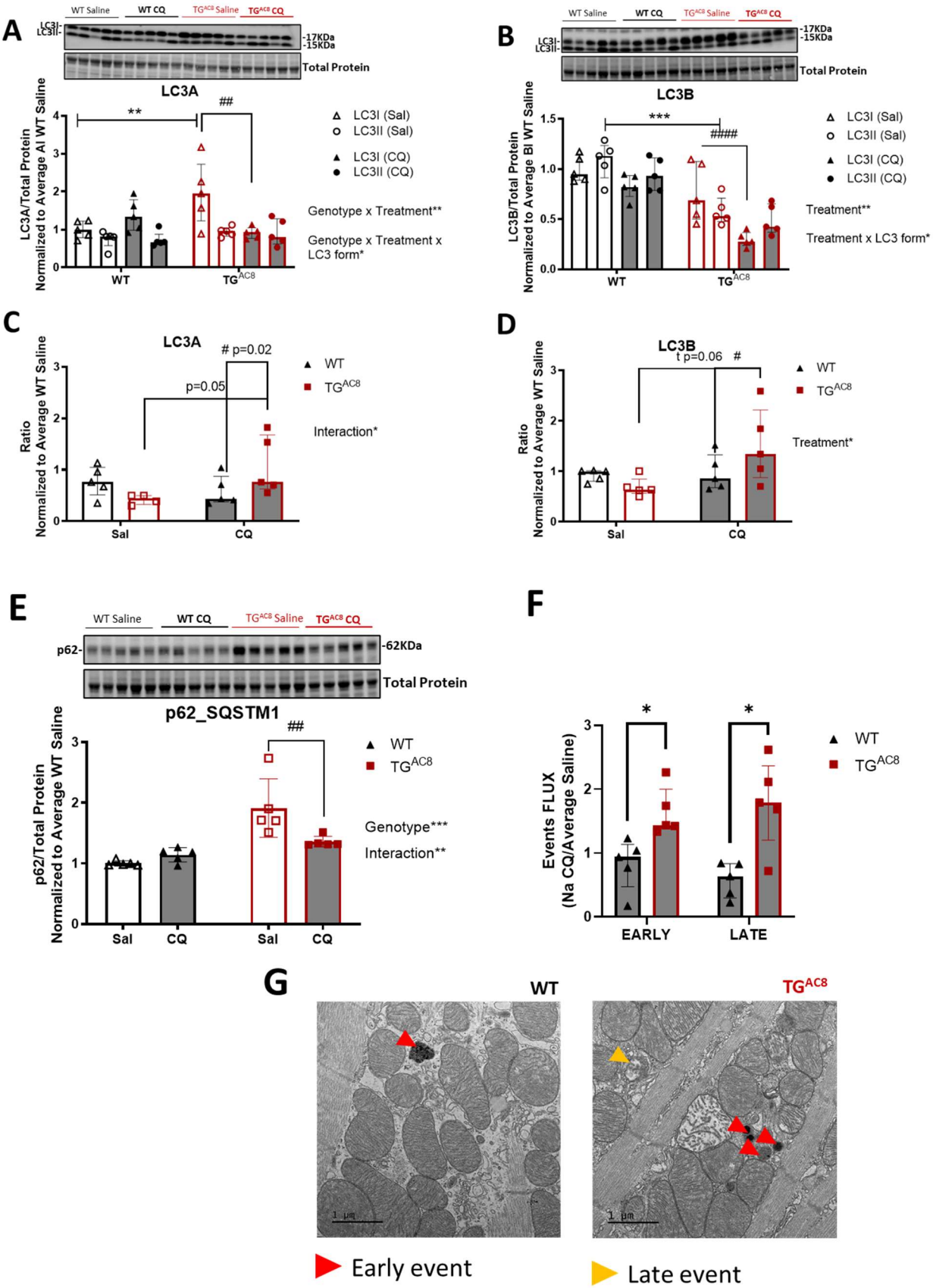
A
WT Saline
WT CQ
TGAC8 Saline
TGAC8 CQ
LC3I-
LC3II-
-17KDa
-15KDa
Total Protein
LC3A
LC3A/Total Protein
Normalized to Average AI WT Saline
**
##
LC3I (Sal)
LC3II (Sal)
LC3I (CQ)
LC3II (CQ)
Genotype x Treatment**
Genotype x Treatment x LC3 form*
WT
TGAC8
B
LC3B
LC3B/Total Protein
Normalized to Average BI WT Saline
***
####
Treatment**
Treatment x LC3 form*
C
LC3A
Ratio
Normalized to Average WT Saline
# p=0.02
p=0.05
Interaction*
Sal
CQ
D
LC3B
t p=0.06 #
Treatment*
E
p62-
-62KDa
p62_SQSTM1
p62/Total Protein
Normalized to Average WT Saline
##
Genotype***
Interaction**
F
Events FLUX
(Na CQ/Average Saline)
*
EARLY
LATE
G
WT
TGAC8
1 µm
Early event
Late event

763 **Figure 4. Autophagic flux is accelerated in TG^{AC8} at 3 months of age.**

764 TG^{AC8} and WT at 3 months of age were treated by intraperitoneal administration of
765 chloroquine (CQ) (50 mg/kg) or saline, and LVs were collected 3 hours after drug
766 administration and snap-frozen for analysis of autophagy markers LC3, LC3II/LC3I ratios,
767 and p62 (n=5 mice per group). Bar graphs and Western blot analysis of **A**), LC3A; **B**),
768 LC3B; **C**), LC3AII/LC3AI; **D**), LC3BII/LC3BI; **E**), p62; **F**), paired TEM event flux
769 quantification of early and late autophagic figures, normalized to average WT saline; **G**)
770 representative micrographs. **A and B**, A three-way ANOVA with repeated measurements,
771 followed by Original FDR method of Benjamini and Hochberg post-hoc multi-comparison
772 test was used. **C, D, E and F**, A two-way ANOVA, followed by Original FDR method of
773 Benjamini and Hochberg post-hoc multi-comparison test was used. Data are presented
774 as the median ± interquartile range.

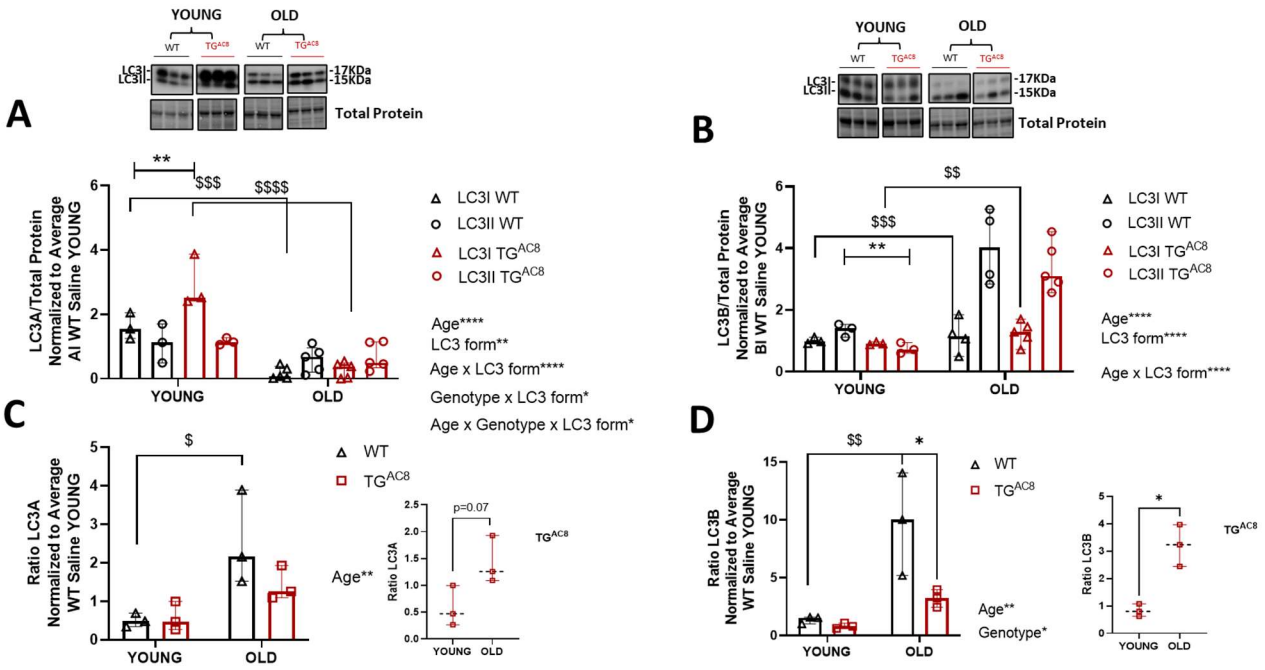
A
YOUNG
OLD
WT
TGAC8
LC3I
LC3II
-17KDa
-15KDa
Total Protein
LC3A/Total Protein Normalized to Average AI WT Saline YOUNG
LC3I WT
LC3II WT
LC3I TGAC8
LC3II TGAC8
Age****
LC3 form**
Age x LC3 form****
Genotype x LC3 form*
Age x Genotype x LC3 form*
B
LC3B/Total Protein Normalized to Average BI WT Saline YOUNG
Age****
LC3 form****
Age x LC3 form****
C
Ratio LC3A Normalized to Average WT Saline YOUNG
WT
TGAC8
Age**
p=0.07
Ratio LC3A
D
Ratio LC3B Normalized to Average WT Saline YOUNG
Age**
Genotype*
Ratio LC3B

775

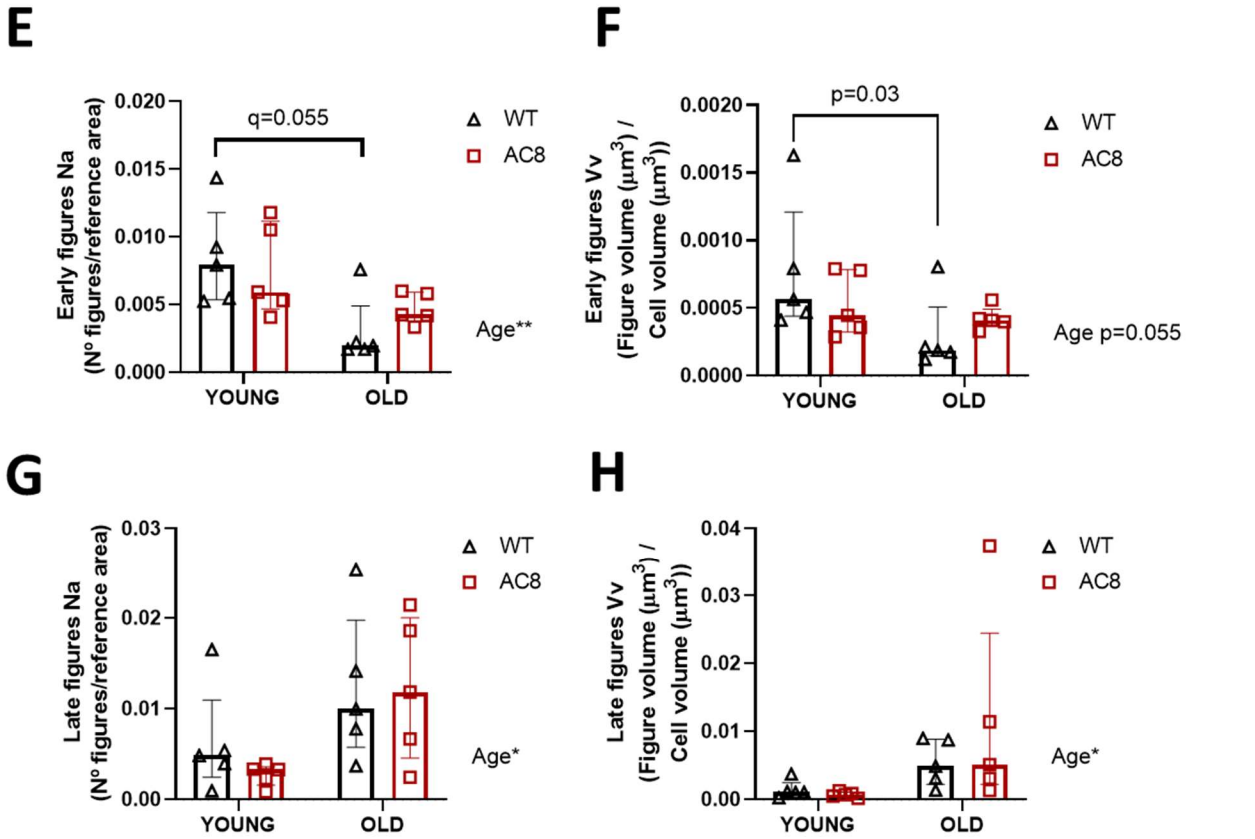
E
Early figures Na (Nº figures/reference area)
q=0.055
WT
AC8
Age**
F
Early figures Vv (Figure volume (µm3) / Cell volume (µm3))
p=0.03
Age p=0.055
G
Late figures Na (Nº figures/reference area)
Age*
H
Late figures Vv (Figure volume (µm3) / Cell volume (µm3))
YOUNG
OLD

776

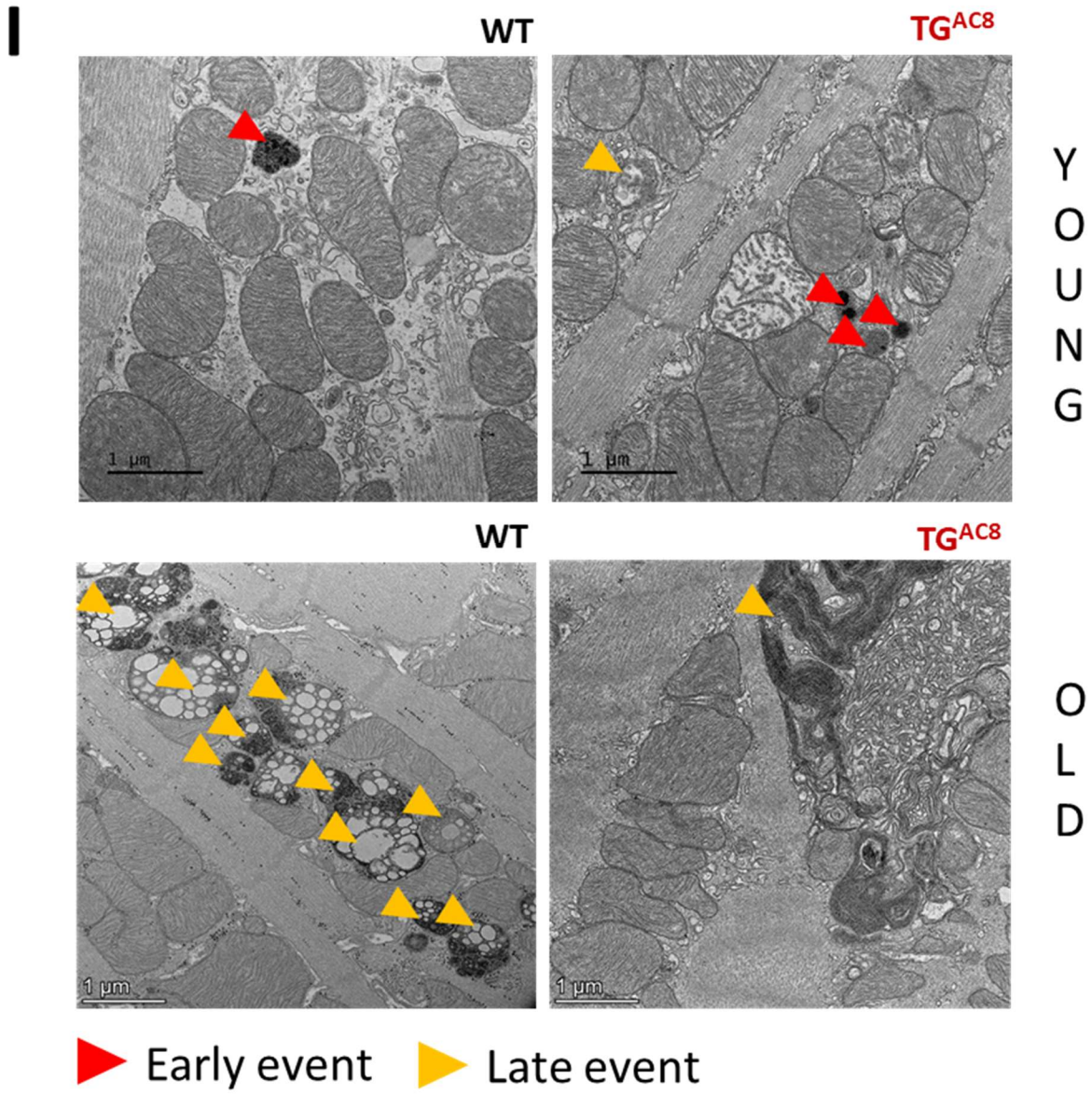

Figure 5. Autophagy decline with aging is independent of genotype.

Bar graphs and Western blot analysis of autophagy markers LC3, LC3II/LC3I ratios and p62 in TG^{AC8} and WT at 3-month (n=3 mice per group) and 21-month of age (n=5 mice per group). **A**), LC3A; **B**), LC3B; **C**), LC3AII/LC3AI ratio; **D**) LC3BII/LC3BI ratio. Bar graphs showing the quantification by TEM of autophagic figures (n=5 mice per group) for *early* events **E**), number of per reference area; **F**) volume per cell volume, and for *late*

events **G**), number of per reference area, **H**) volumes per cell volume. **I**, TEM representative images. **A and B**, A three-way ANOVA with repeated measurements, followed by Original FDR method of Benjamini and Hochberg post-hoc multi-comparison test was used. **C, D, E, F, G and H**, A two-way ANOVA, followed by Original FDR method of Benjamini and Hochberg post-hoc multi-comparison test was used. Data are presented as the median ± range in A and B, and as median ± interquartile range in all others.

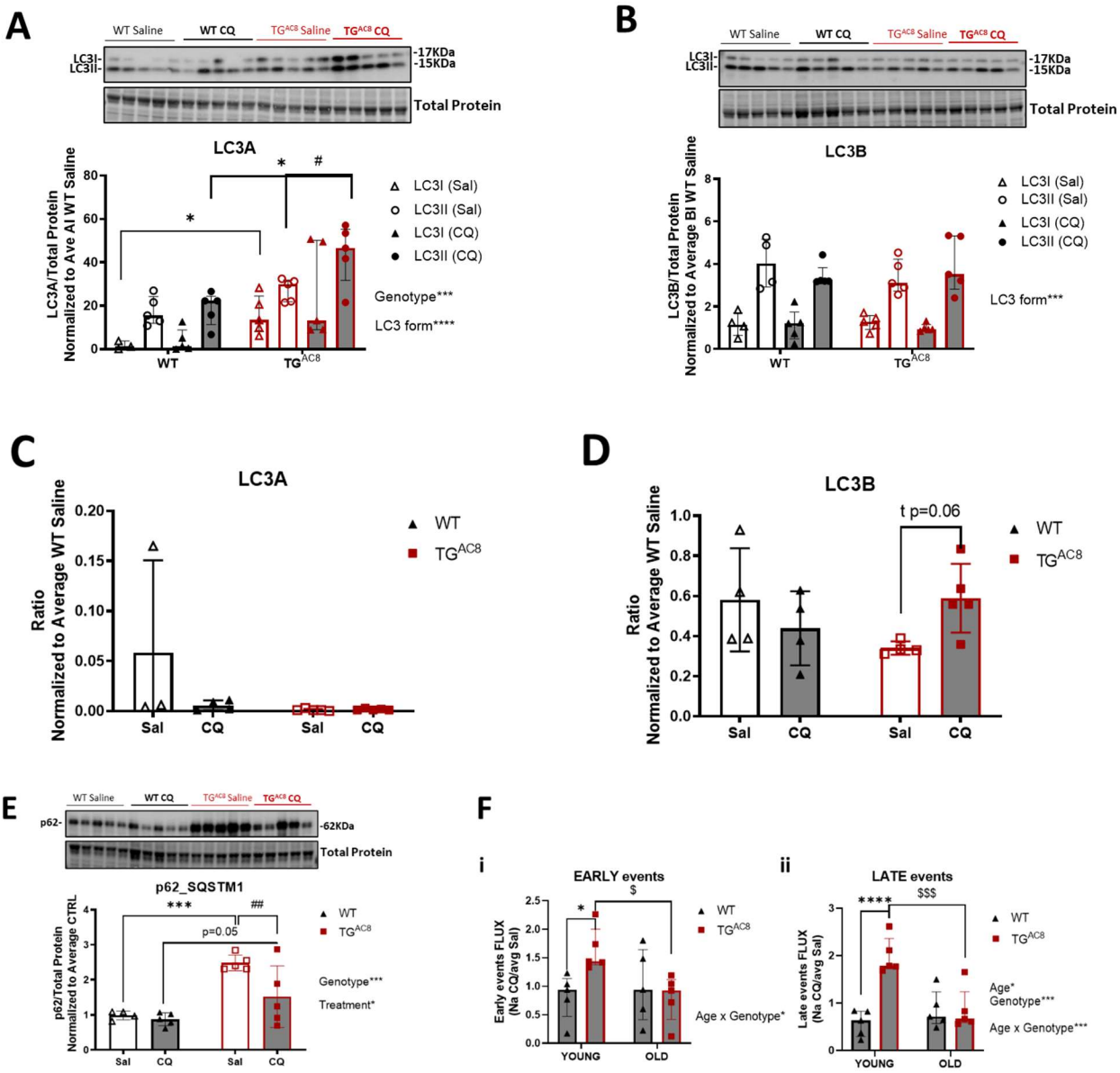

Figure 6. Accelerated autophagic flux in young TG^{AC8} heart becomes maladaptive and insufficient in old age.

TG^{AC8} and WT littermates at 21 months of age were treated by intraperitoneal administration chloroquine (CQ) (50 mg/kg) or saline, and LVs (n=5 mice per group) were collected 3 hours after and snap-frozen for analysis of autophagy markers LC3 and p62. Bar graphs and Western blot analysis of **A**), LC3A; **B**), LC3B; **C**), LC3AII/LC3AI ratio; **D**), LC3BII/LC3BI ratio; **E**), total p62. **F**), paired TEM micrograph quantification of early (**i**)

800 and late (**ii**) autophagic figures, normalized to average WT saline (n=5 mice per group).
801 **A and B**, A three-way ANOVA with repeated measurements, followed by Original FDR
802 method of Benjamini and Hochberg post-hoc multi-comparison test was used. **C, D, E**
803 **and F**, A two-way ANOVA, followed by Original FDR method of Benjamini and Hochberg
804 post-hoc multi-comparison test was used. Data are presented as the median ±
805 interquartile range.

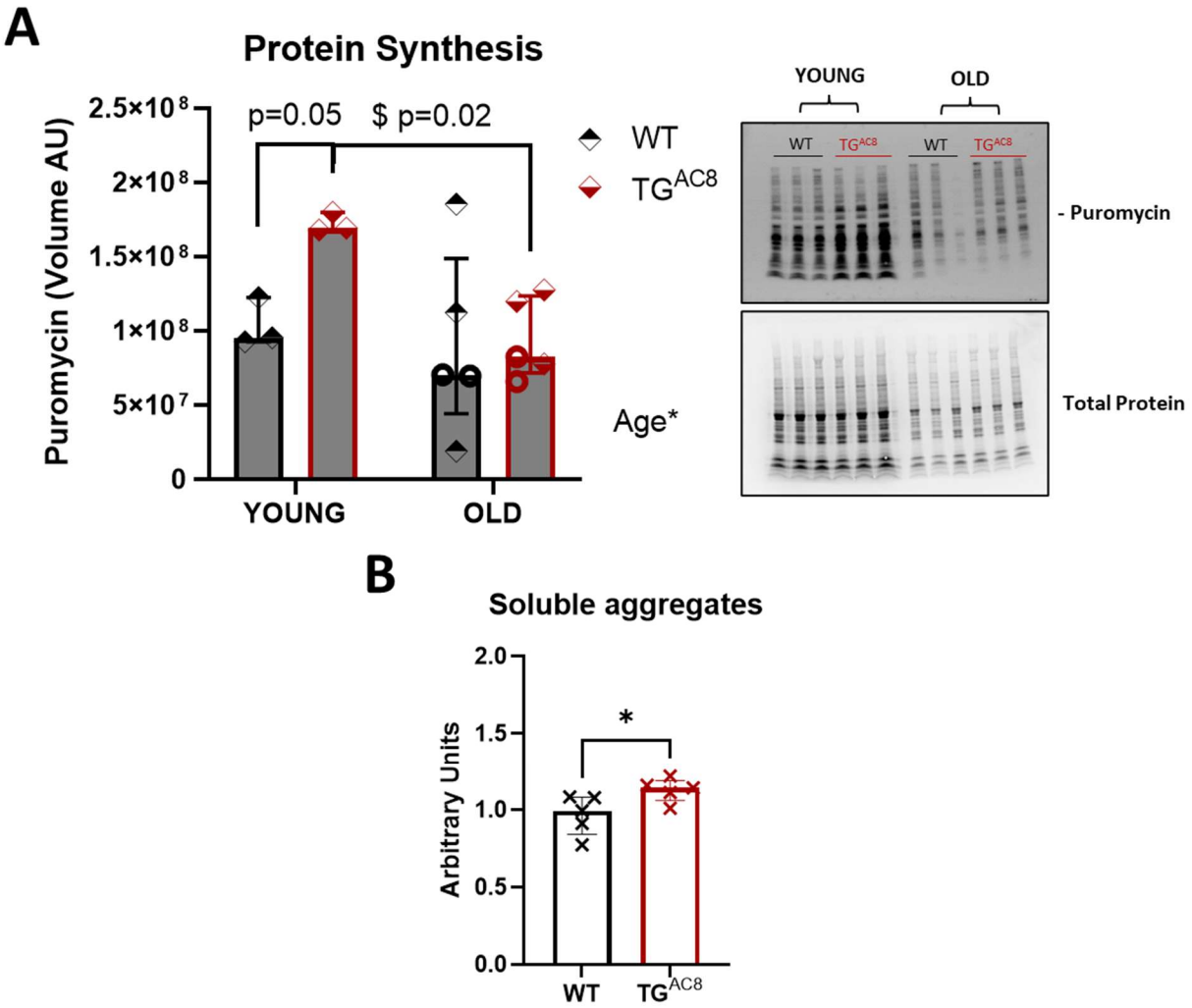
A
Protein Synthesis
Puromycin (Volume AU)
2.5×10^8
2×10^8
1.5×10^8
1×10^8
5×10^7
0
p=0.05
$ p=0.02
YOUNG
OLD
WT
TG^AC8
Age*
YOUNG
OLD
WT
TG^AC8
WT
TG^AC8
- Puromycin
Total Protein
B
Soluble aggregates
Arbitrary Units
2.0
1.5
1.0
0.5
0.0
*
WT
TG^AC8

806

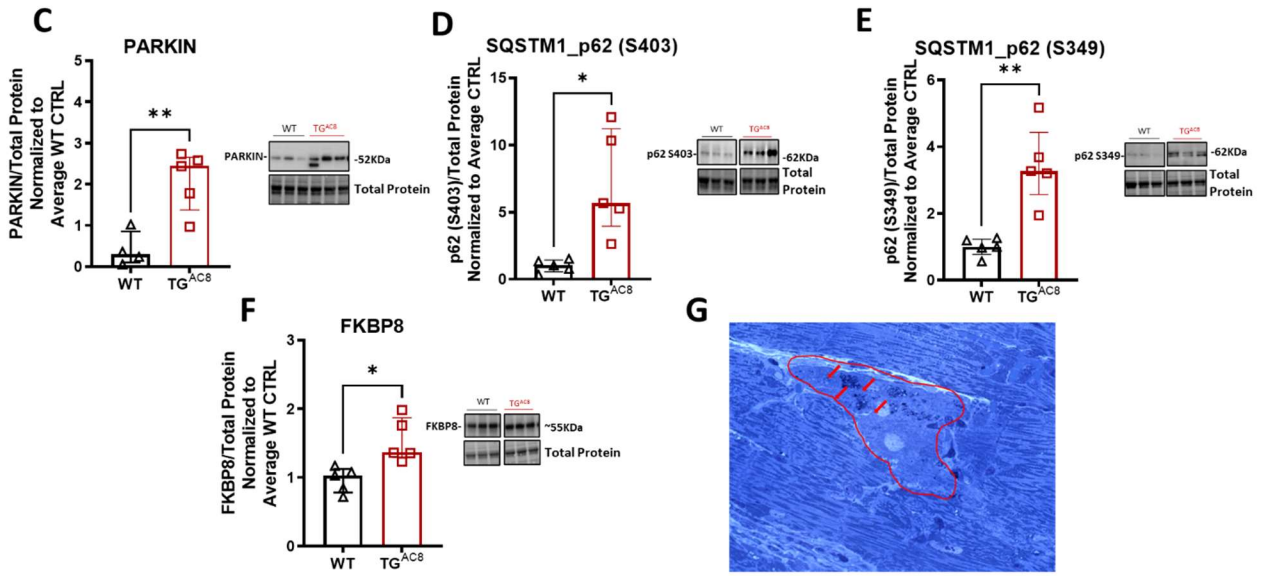
C
PARKIN
PARKIN/Total Protein Normalized to Average WT CTRL
**
WT
TG^AC8
PARKIN-
-52KDa
Total Protein
D
SQSTM1_p62 (S403)
p62 (S403)/Total Protein Normalized to Average CTRL
*
WT
TG^AC8
p62 S403-
-62KDa
Total Protein
E
SQSTM1_p62 (S349)
p62 (S349)/Total Protein Normalized to Average CTRL
**
WT
TG^AC8
p62 S349-
-62KDa
Total Protein
F
FKBP8
FKBP8/Total Protein Normalized to Average WT CTRL
*
WT
TG^AC8
FKBP8-
~55KDa
Total Protein
G

807

808 **Figure 7. Proteostasis is deregulation is more severe in old TG^{AC8} heart.**

809 **A**), TG^{AC8} and WT at 19 months of age (n=5 mice per group) were treated by
810 intraperitoneal administration of puromycin (0.022g/g mouse) according to the SUnSET
811 method, and LVs were collected 30 minutes after drug administration and snap-frozen for
812 puromycin analysis. Bar graphs and Western blot analysis of **B**), Aggresome
813 quantification in soluble fractions (n=6 mice per group, old TG^{AC8} and WT at 17-18 months
814 of age); mitophagy canonical cargo receptors (n=5 mice per group, old TG^{AC8} and WT at
815 21 months of age) **C**), PARKIN; **D**), SQSTM1_p62-S403; **E**), SQSTM1_p62-S349 and the
816 noncanonical cargo receptor **F**) FKBP8. **G**), Semithin staining of old TG^{AC8} LV showing
817 mitochondrial loss of structure. A two-way ANOVA, followed by Original FDR method of
818 Benjamini and Hochberg post-hoc multi-comparison test was used for **A**. Unpaired 2-
819 tailed Student t test with Welch's correction was used for **B, C, D**, **E, and F**. Data are
820 presented as the median ± interquartile range.

Severe proteostasis disruption leads the old TG^{AC8} heart to accelerated aging

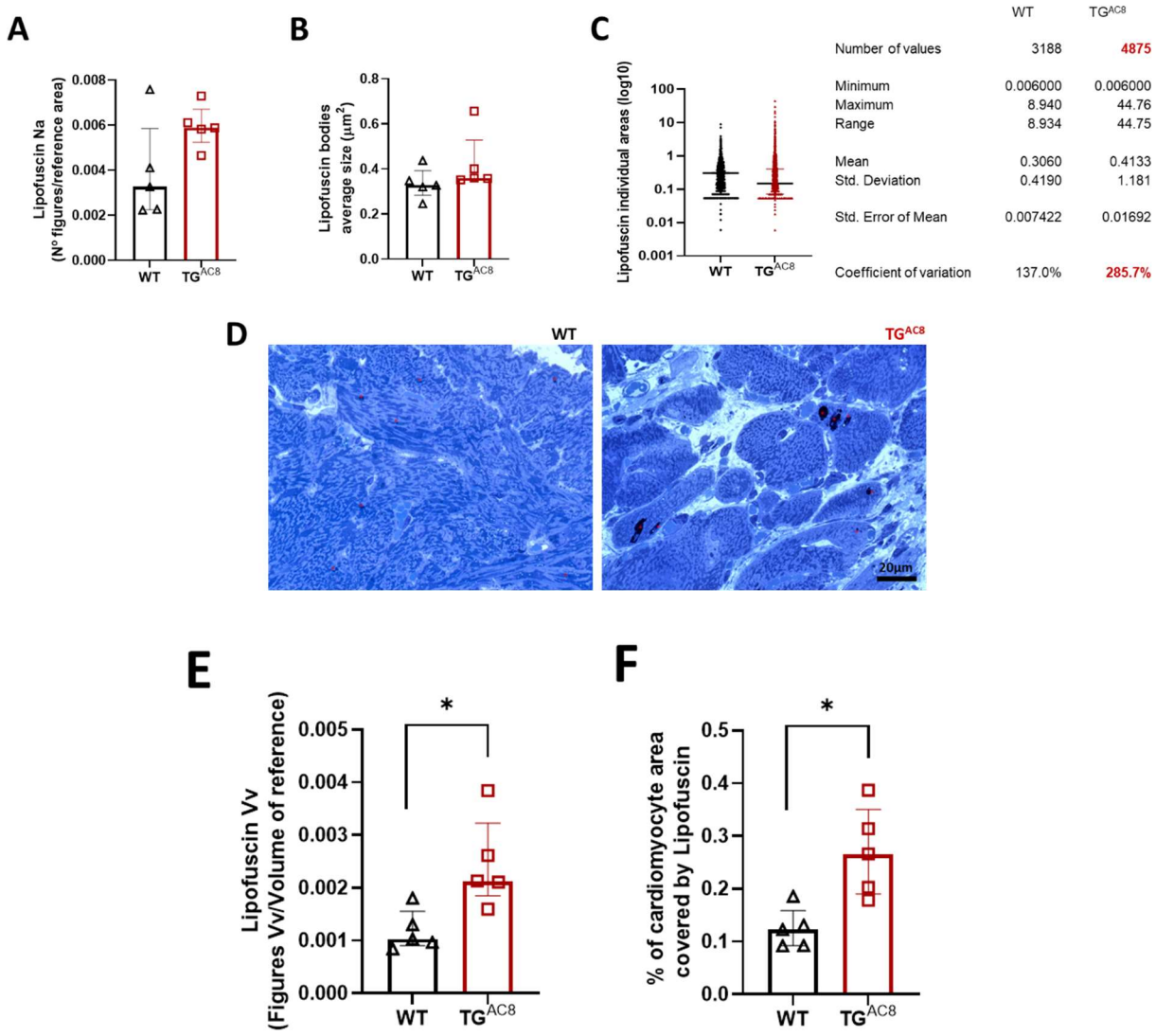

	WT	TG^{AC8}
Number of values	3188	4875
Minimum	0.006000	0.006000
Maximum	8.940	44.76
Range	8.934	44.75
Mean	0.3060	0.4133
Std. Deviation	0.4190	1.181
Std. Error of Mean	0.007422	0.01692
Coefficient of variation	137.0%	285.7%

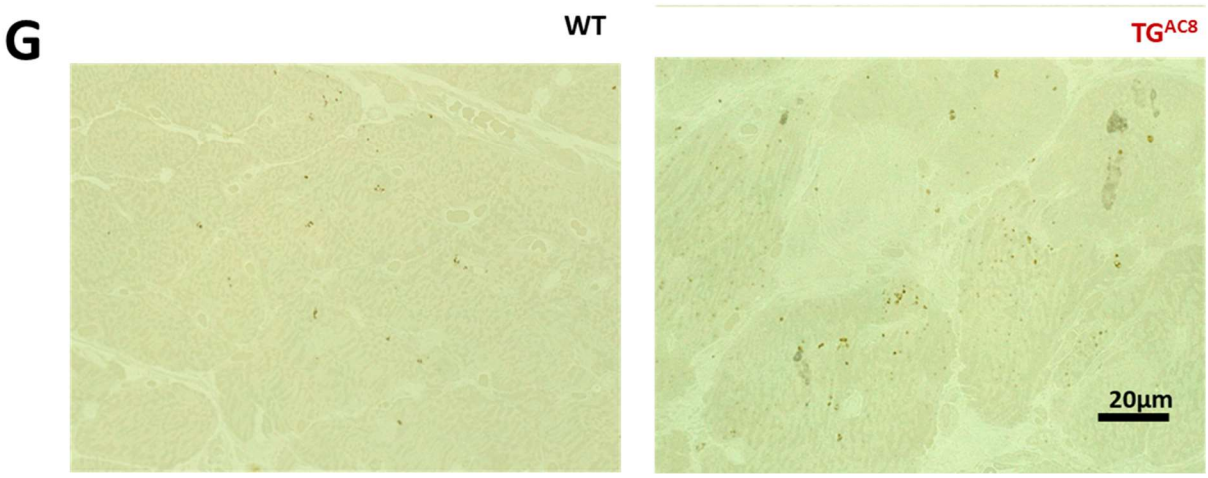

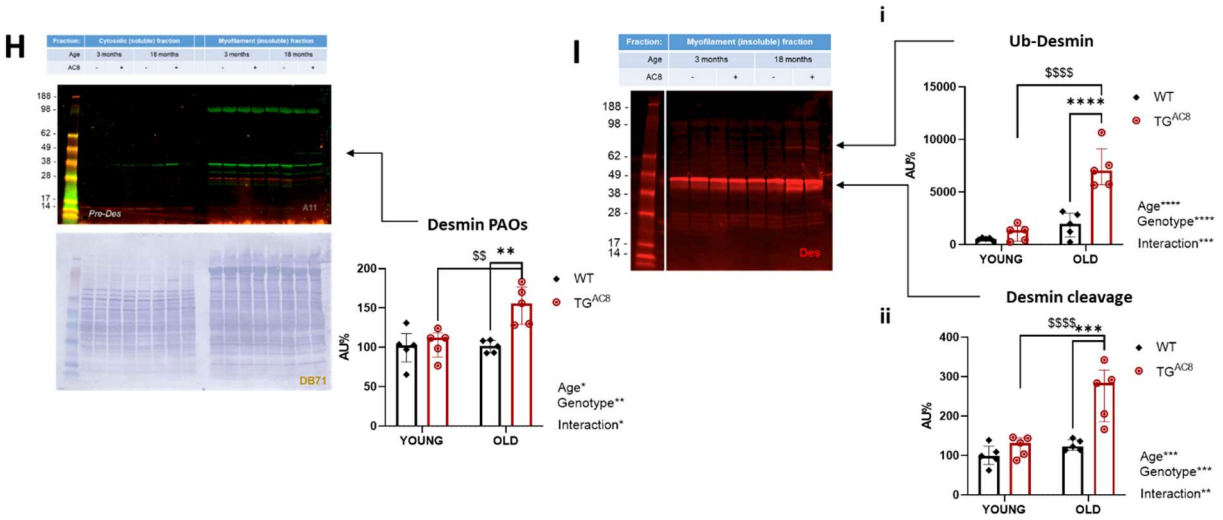

Figure 8. Proteostasis dysregulation by PQC insufficiency leads to increased lipofuscin accumulation and deposition of desmin Pre-Amyloid Oligomers (PAOs) contributing to TG^{AC8} accelerated aging.

Bar graphs representing the quantification of undigested material (LF and desmin) in old TG^{AC8} and WT (n=5 per group); **A**), number of figures per reference area; **B**), average size of lipofuscin bodies; **C**), violin plot showing the more aberrant sizes of lipofuscin bodies; **D**), Representative semi-thin staining of lipofuscin bodies; **E**), volume of figures per volume of reference area; **F**) percentage of cardiomyocyte area covered by lipofuscin; **G**), Representative image of Palade staining of TEM semi-thin sections showing the presence of brown to black pigments in old TG^{AC8} and age-matched WT; **H**), soluble and insoluble (myofilament-enriched) fractions probed with the A11 antibody for pre-amyloid oligomers (top), and total protein staining (Direct Blue71, DB71), with relative densitometry analysis; **I**), insoluble (myofilament-enriched) fractions probed with the desmin antibody, and relative densitometry for **i**) ubiquitinated and **ii**) cleaved desmin proteoforms, in old TG^{AC8} age-matched WT. **A, B**, **C, E**, **and F**, Unpaired 2-tailed Student t test with Welch's correction was used; **L and M**, A two-way ANOVA, followed by Original

840 FDR method of Benjamini and Hochberg post-hoc multi-comparison test was used. Data

841 are presented as the median ± interquartile range.

842 # SUPPLEMENTAL MATERIAL

843 Table S1

S1

Protein Name	Symbol	log2(average expression)	log2(fold change)	p-value
Lysosomal protective protein	Ctsa	0.017702383	0.216799716	0.004513026
Cathepsin B	Ctsb	0.022381593	0.120723106	0.0254094
Dipeptidyl peptidase 1	Ctsc	0.033052876	0.167723218	0.028205766
Cathepsin D	Ctsd	0.011868307	0.164671994	0.033523037
Cathepsin F	Ctsf	0.011385877	0.134158334	0.03797905
Pro-cathepsin H	Ctsh	-0.032543079	0.171483139	0.115212134
Cathepsin L1	Ctsl	-0.002089995	0.082015669	0.037159714
Cathepsin S	Ctss	0.028762851	0.317183952	0.007053072
Cathepsin Z	Ctsz	0.014751699	0.403327276	0.008561447

844

845 **Table S1. Relative cathepsin expression in TG^{AC8} at 3 months of age.**

846 ProteOMICs data in TG^{AC8} at 3 months (n=4 mice per group).

847 Figures S1–S5

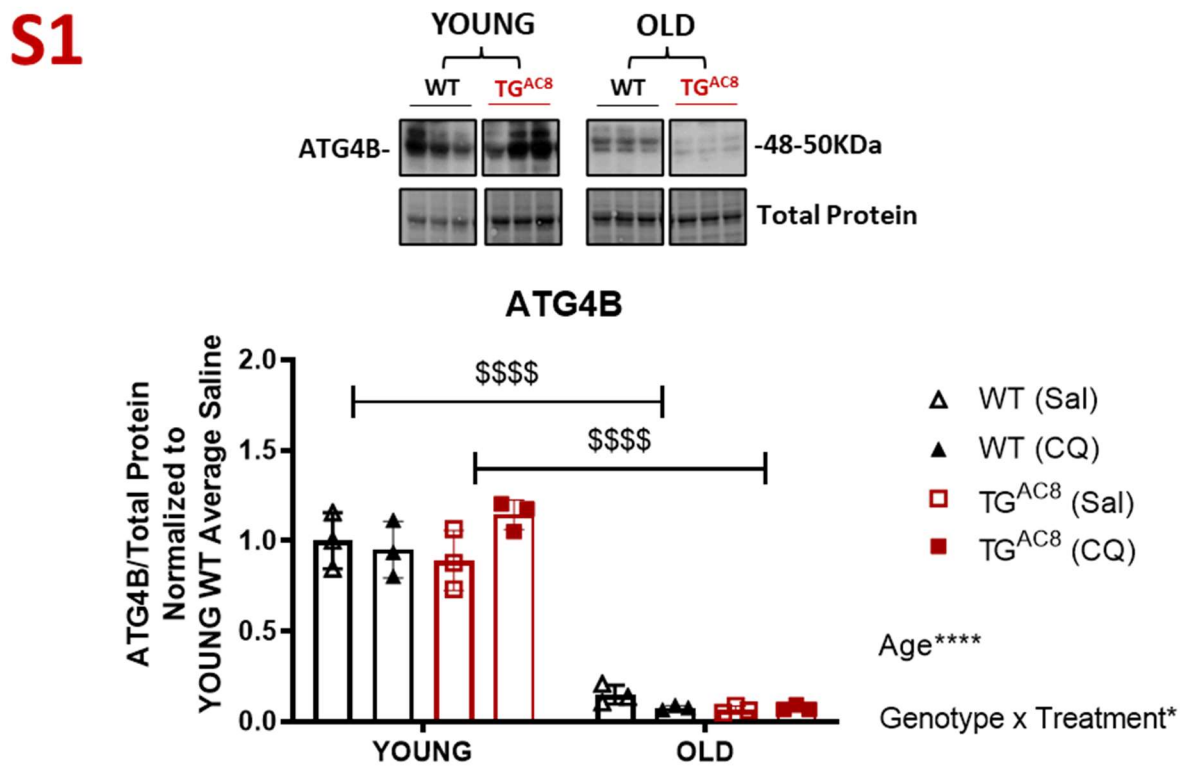

848

849 **Figure S1. ATG4B expression with aging in TG^{AC8} and WT LVs.**

850 Bar graphs and Western blot analysis of ATG4B in TG^{AC8} and WT littermates LVs at 3

851 months and 21 months of age (n=3 mice per group). A three-way ANOVA followed by

852 Original FDR method of Benjamini and Hochberg post-hoc multi-comparison test was

853 used. Data are presented as the median ± range.

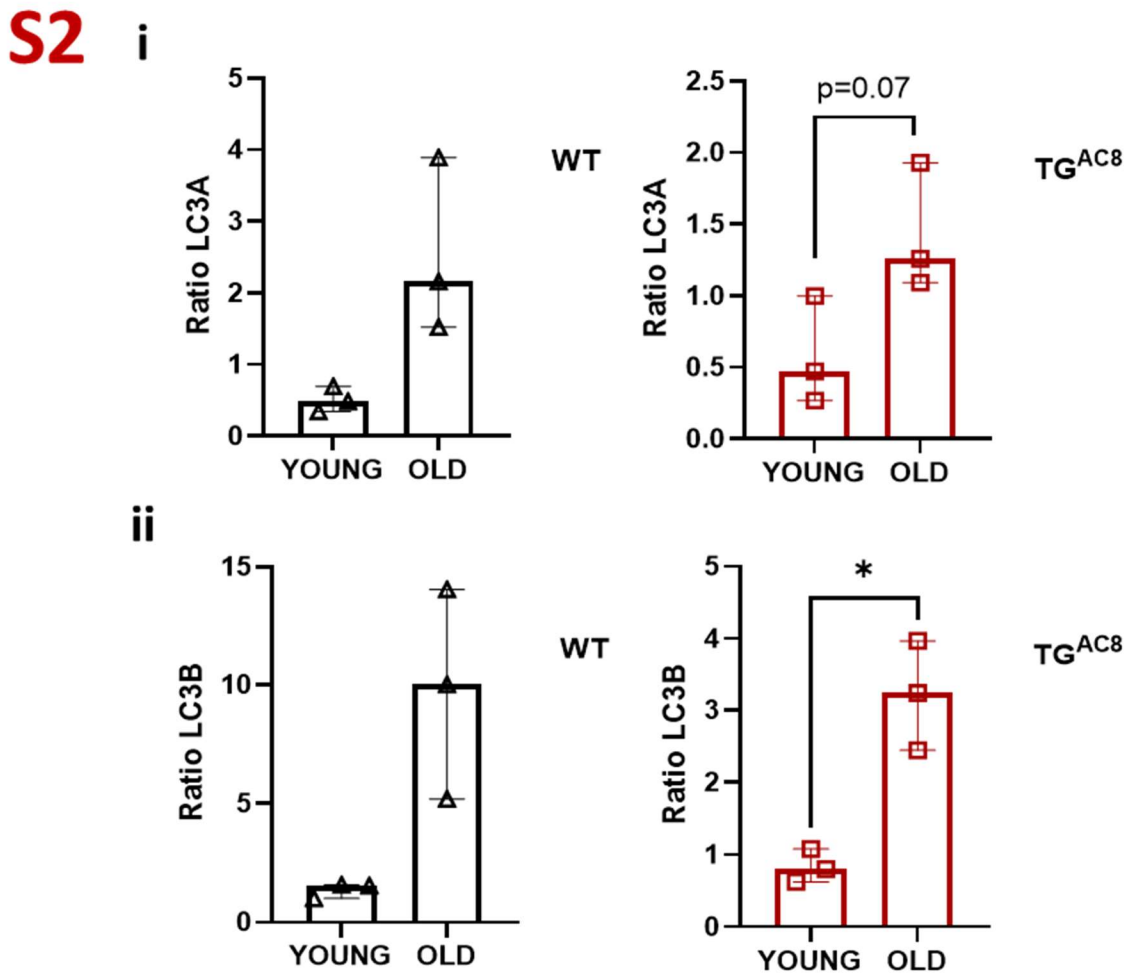

854

855 **Figure S2. LC3II/LC3I ratios with aging in TG^{AC8} and WT at 21 vs 3 months.**

856 Bar graphs and Western blot analysis of LC3II/LC3I ratios in young (3 months) and old

857 (21 months) WT and TG^{AC8} LVs (n=3 mice per group). **i**) LC3AII/LC3AI ratio; **ii**),

858 LC3BII/LC3BI ratio. Unpaired 2-tailed Student t test with Welch's correction was used.

859 Data are presented as the median ± interquartile range.

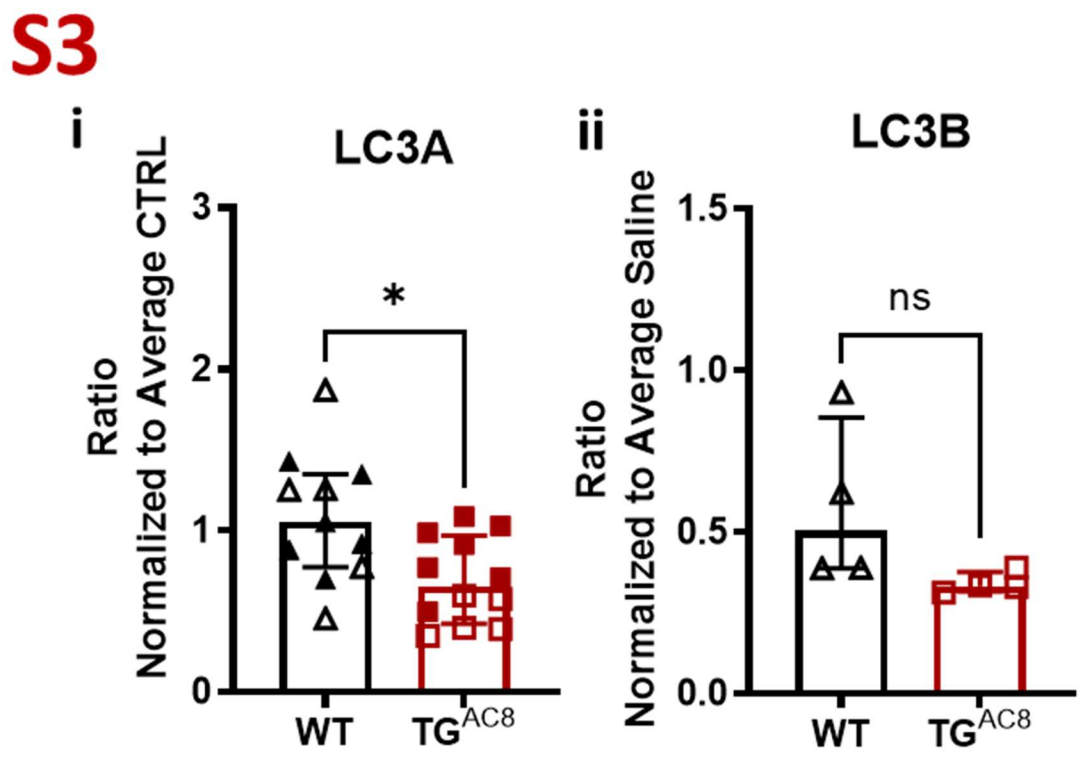

Figure S3. LC3AII/LC3AI ratio is significantly downregulated in old TG^{AC8} similar to 3-months of age.

Bar graphs and Western blot analysis of LC3II/LC3I ratios in old (21 months) WT and TG^{AC8} LVs. **i**) LC3AII/LC3AI ratio (n=11 mice in the WT group, n=12 mice in the TG^{AC8} group); **ii**) LC3BII/LC3BI ratio (n=5 mice per group). Unpaired 2-tailed Student t test with Welch's correction was used. Data are presented as the median ± interquartile range.

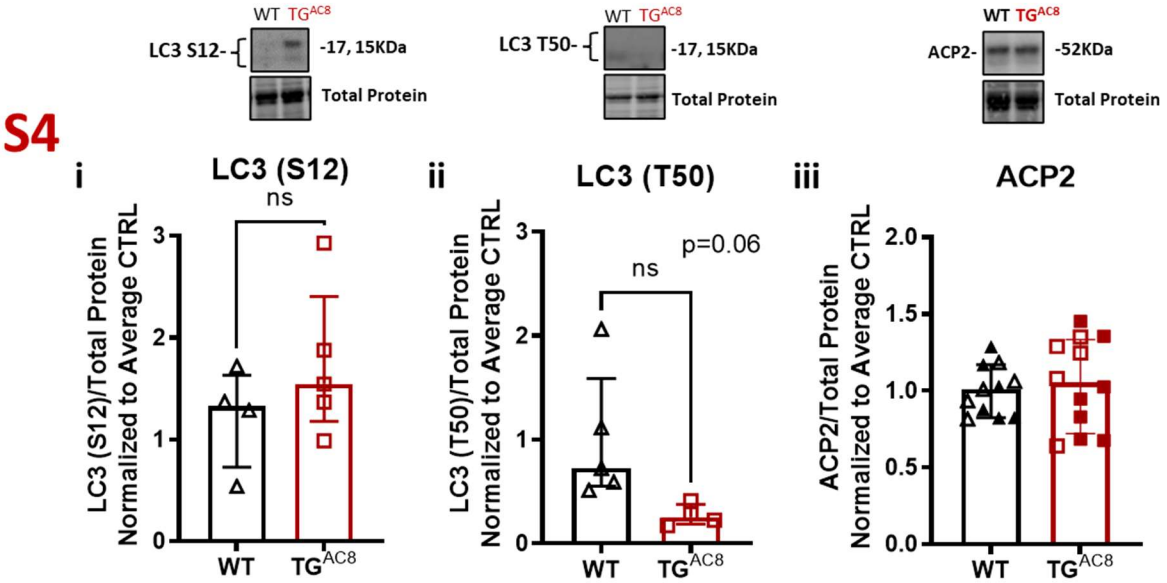

867

868 **Figure S4. Autophagy marker expression in old TG^{AC8} and WT at 21 months.**

869 Bar graphs and Western blot analysis of LC3 phospho-forms and the lysosomal hydrolase

870 ACP2 in old TG^{AC8} and WT LVs at 21 months of age. **i**), LC3-S12 and **ii**) LC3-T50 (n=5

871 mice per group); **iii**), ACP2 (n=11 mice WT group, n=12 mice TG^{AC8} group. Unpaired 2-

872 tailed Student t test with Welch's correction was used in **A and B**. Unpaired 2-tailed

873 Student t test was used in **C**. Data are presented as the median ± interquartile range.

S5

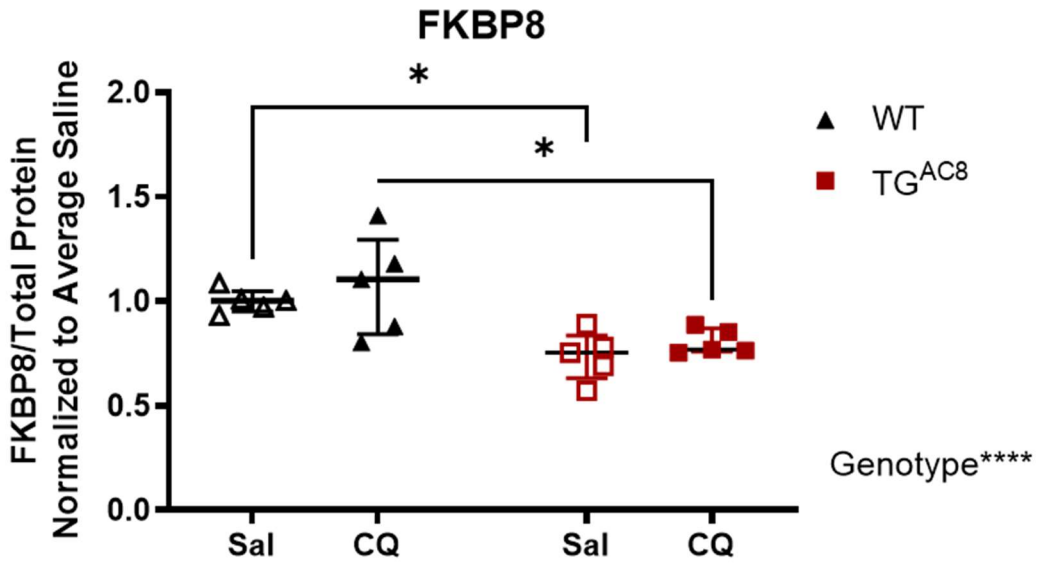

874

875 **Figure S5. Non-canonical mitophagy receptor FKBP8 is decreased in TG^{AC8} at 3**
876 **months.**

877 TG^{AC8} and WT littermates at 3 months of age were treated by intraperitoneal
878 administration chloroquine (CQ) (50 mg/kg) or saline, and LVs (n=5 mice per group) were
879 collected 3 hours after and snap-frozen for analysis of the non-canonical mitophagy
880 receptor FKBP8 A two-way ANOVA, followed by Original FDR method of Benjamini and
881 Hochberg post-hoc multi-comparison test was used. Data are presented as the median ±
882 interquartile range.